Downloaded from gsabulletin.gsapubs.org on December 30, 2009

Geological Society of America Bulletin

Ground-water sapping processes, Western Desert, Egypt

Wei Luo, Raymond E. Arvidson, Mohamed Sultan, Richard Becker, Mary Katherine Crombie, Neil Sturchio and Zeinhom El Alfy

Geological Society of America Bulletin 1997;109;43-62
doi: 10.1130/0016-7606(1997)109<0043:GWSPWD>2.3.CO;2

Email alerting services click www.gsapubs.org/cgi/alerts to receive free e-mail alerts when new articles cite this article

Subscribe click www.gsapubs.org/subscriptions/ to subscribe to Geological Society of America Bulletin

Permission request click http://www.geosociety.org/pubs/copyrt.htm#gsa to contact GSA

Copyright not claimed on content prepared wholly by U.S. government employees within scope of their employment. Individual scientists are hereby granted permission, without fees or further requests to GSA, to use a single figure, a single table, and/or a brief paragraph of text in subsequent works and to make unlimited copies of items in GSA's journals for noncommercial use in classrooms to further education and science. This file may not be posted to any Web site, but authors may post the abstracts only of their articles on their own or their organization's Web site providing the posting includes a reference to the article's full citation. GSA provides this and other forums for the presentation of diverse opinions and positions by scientists worldwide, regardless of their race, citizenship, gender, religion, or political viewpoint. Opinions presented in this publication do not reflect official positions of the Society.

Notes

Geological Society of America

THE GEOLOGICAL SOCIETY OF AMERICA

Downloaded from gsabulletin.gsapubs.org on December 30, 2009

Ground-water sapping processes, Western Desert, Egypt

Wei Luo*
Raymond E. Arvidson
Mohamed Sultan
Richard Becker
Mary Katherine Crombie
McDonnell Center for the Space Sciences, Department of Earth and Planetary Sciences, Washington University, St. Louis, Missouri 63130

Neil Sturchio *Argonne National Laboratory, Argonne, Illinois 60439*

Zeinhom El Alfy *Egyptian Geological Survey and Mining Authority, Cairo, Egypt*

ABSTRACT

Depressions of the Western Desert of Egypt (specifically, Kharga, Farafra, and Kurkur regions) are mainly occupied by shales that are impermeable, but easily erodible by rainfall and runoff, whereas the surrounding plateaus are composed of limestones that are permeable and more resistant to fluvial erosion under semiarid to arid conditions. Scallop-shaped escarpment edges and stubby-looking channels that cut into the plateau units are suggestive of slumping of limestones by ground-water sapping at the limestone-shale interfaces, removal of slump blocks by weathering and fluvial erosion, and consequent scarp retreat. Spring-derived tufa deposits found near the limestone escarpments provide additional evidence for possible ground-water sapping during previous wet periods. A computer simulation model was developed to quantify the ground-water sapping processes, using a cellular automata algorithm with coupled surface runoff and ground-water flow for a permeable, resistant layer over an impermeable, friable unit. Erosion, deposition, slumping, and generation of spring-derived tufas were parametrically modeled. Simulations using geologically reasonable parameters demonstrate that relatively rapid erosion of the shales by surface runoff, ground-water sapping, and slumping of the limestones, and detailed control by hydraulic conductivity inhomogeneities associated with structures explain the depressions, escarpments, and associated landforms and deposits. Using episodic wet pulses, keyed by $\delta^{18}O$ deep-sea core record, the model produced tufa ages that are statistically consistent with the observed U/Th tufa ages. This result supports the hypothesis that northeastern African wet periods occurred during interglacial maxima. The $\delta^{18}O$-forced model also replicates the decrease in fluvial and sapping activity over the past million years, as northeastern Africa became hyperarid. The model thus provides a promising predictive tool for studying long-term landform evolution that involves surface and subsurface processes and climatic change.

INTRODUCTION

Among the most prominent geomorphic features of the current hyperarid Western Desert of Egypt are a series of depressions surrounding plateaus and escarpments. The escarpments extend for hundreds of kilometers (Fig. 1). The depressions are largely floored by shales, whereas the surrounding plateaus are composed mainly of limestones (Hermina, 1990). Previous models for the origin of these landforms include wind erosion (Ball, 1927), fluvial erosion (Said, 1983; McCauley et al., 1982), and ground-water sapping (e.g., Maxwell, 1982; Higgins, 1990). Wind alone cannot erode the resistant limestone caprock. Fluvial erosion alone cannot explain some peculiar geomorphic features, such as scalloped escarpments and large depressions. For the depressions and escarpments of the Western Desert, we believe that fluvial erosion and ground-water sapping working together offer the best explanation (e.g., Maxwell, 1982; Issar, 1982; Higgins, 1990). Furthermore, these processes were much more important in the past as compared with today. For example, McCauley et al. (1982, 1986) were able to identify the presence of a relict, buried drainage network in the eastern Sahara by using Shuttle Imaging Radar (SIR) images.

Ground-water sapping is the process that causes entrainment of soil or rock when ground-water flows through and emerges from a porous medium at a free slope surface. This leads to shear strength loss of the basal support and Coulomb failure of the overlying rock (Dunne, 1990; Uchupi and Oldale, 1994; Schumm et al., 1995). Characteristic requirements for ground-water sapping include a permeable aquifer, a rechargeable ground-water system, a free face at which subsurface water can emerge, and a means of transporting material released from the scarp face (Laity, 1988). Structural control through high hydraulic conductivity faults is also typical (Laity, 1988). Sapping processes produce channels that migrate headward into escarpments, with steep sides, flat floors, and theater-like heads that lack well-developed tributaries (Laity and Malin, 1985; Kochel and Piper, 1986; Uchupi and Oldale, 1994).

The objective of this paper is to gather and integrate evidence to explore quantitatively the hypothesis that escarpments and depressions of the Western Desert were caused by fluvial and sapping processes. The procedure followed is to first establish a qualitative conceptual model for the processes involved, using published work, remote sensing, and field observations to provide constraints. The next step is to quantify the primary processes with a numerical computer model that integrates the evidence into an overall landform evolution system that includes coupled fluvial and sapping processes. The modeling approach provides insights into the processes that are no longer operating in the study area.

*Present address: Department of Geography, Northern Illinois University, DeKalb, Illinois 60115. E-mail address: luo@taiga.geog.niu.edu.

Data Repository item 9636 contains additional material related to this article.

GSA Bulletin; January 1997; v. 109; no. 1; p. 43–62; 21 figures; 2 tables.

Downloaded from gsabulletin.gsapubs.org on December 30, 2009

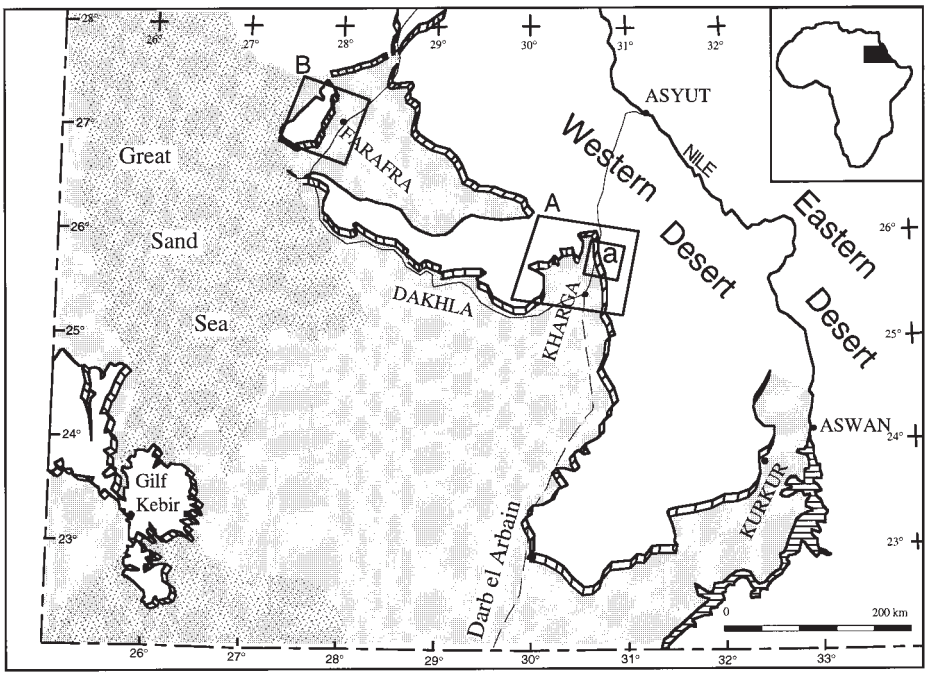

Figure 1. Location map of Western Desert, Egypt, showing major depressions (dark stipple areas), plateaus, and aeolian sand deposits. Escarpments bordering the depressions extend for hundreds of kilometers. Box a denotes the study area shown in Figures 3 and 6. Boxes A and B denote footprints of Thematic Mapper data and Système Probatoire d'Observation de la Terre (SPOT) data shown in Figures 5 and 11, respectively. Study areas visited in the field include the Kharga, Farafra, and Kurkur regions (adapted from Hermina, 1990).

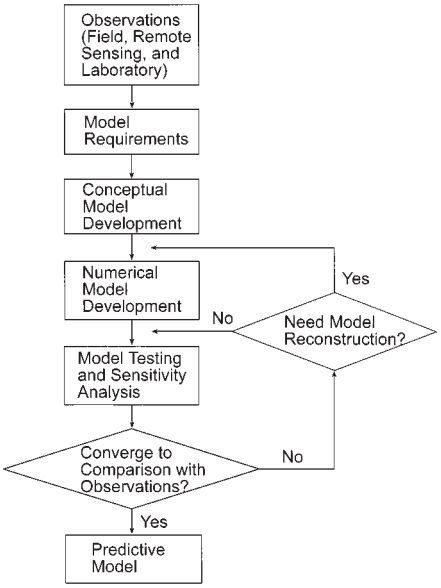

Figure 2. Flow diagram of the modeling approach of this study. The parameter values are selected based on independent measurements documented in the literature if possible. The model was used to estimate the few parameters that have no independent constraint by comparing model outputs with the observations. The result is a predictive model that can provide insights into processes that are no longer operating.

The approach is summarized in a flow diagram shown in Figure 2. The paper focuses on the Kharga and Farafra regions, because these two areas were visited by us in 1994 and 1995. An additional site, the Kurkur Oasis, was also visited by us in 1995 and results were reported in Crombie et al. (1995, 1997). The Kurkur Oasis setting is similar to the ones found at the Kharga and Farafra areas. Thus, a detailed discussion of the Kurkur region will not be developed in this paper.

OBSERVATIONS

Geology and Morphology

Kharga Region. *Observations.* The Kharga depression is ≈200 km north to south and ≈70 km east to west (Fig. 1). It is bounded by steep escarpments and plateaus on all but the southern side. The elevation of the depression is about 50 m above sea level; the plateau is about 400 m above sea level (Defense Mapping Agency Topographic Center, 1972). The strata are almost horizontal, with 1° to 2° dips to the west-southwest and to the east-northeast; the depression is oriented along a north-south–trending anticline (Said, 1962). Figure 3 is a simplified geologic map for part of the Kharga study area, called El Rufuf Pass, which we examined in 1994. Figure 4 shows representative cross sections. El Rufuf Pass is the site of a major fault system striking northeast-southwest. Spring- and wadi-related tufa deposits crop out along and close to the escarpments, providing direct evidence for emergent ground-water in the past (Caton-Thompson and Gardner, 1932; Stringfield et al., 1974).

The Kharga depression is floored by the Maghrabi, Quseir, and Dakhla formations. The oldest unit exposed is the Maghrabi Formation (Cretaceous), which consists of coastal mudplain deposits and channel sandstones, deltaic and marginal marine sandstones and mudstones, and paleosol deposits. The thickness of this formation is ≈60 m (Hermina; 1990; Handley et al., 1987). The Quseir Formation consists of shale, claystones, siltstones, and flaggy sandstones with a thickness up to ≈70–90 m (Hermina, 1990). The Dakhla Formation is primarily composed of shale in the study area, with minor intercalations of calcareous, sandy and silty deposits. To the east of these outcrops is a small plateau underlain by the Tarawan Formation, a unit composed of white neritic chalk and chalky limestone of Paleocene age, having a thickness of as much as ≈45 m (Hermina; 1990, Handley et al., 1987). Farther to the east is the major escarpment. The Esna Formation is exposed at the base of the escarpment and consists of primarily marl and green shales, enclosing minor carbonate intercalations. The thickness reaches ≈160 m and decreases toward the south (Hermina, 1990; Handley et al., 1987). Overlying the Esna Formation and forming the large plateau is a sequence of predominantly carbonate rocks called the Thebes Group. In the study area, the Thebes Group is represented by the El Rufuf Formation, which consists of well-bedded lagoonal to platform limestones of early Eocene age, with a maximum thickness of 145 m (Hermina; 1990, Handley et al., 1987). The El Rufuf Formation forms the caprock of the plateau surrounding the Kharga depression in the region shown in Figure 3.

Figure 5 is a regional view from Landsat Thematic Mapper (TM) band 5 (1.55–1.75 μm in wavelength) showing the topographic contrast of depressions and escarpments. Extensive aeolian streaks, which are most obvious in the middle portion of Figure 5, indicate the current hyperarid conditions (average annual rainfall <1 mm, Wendorf and Schild, 1980). Numerous escarpments are evident, including stubby channel systems that cut into the Tarawan Formation and scalloped forms that cut into the El Rufuf Formation. Figure 6 shows the study area with TM

Downloaded from gsabulletin.gsapubs.org on December 30, 2009

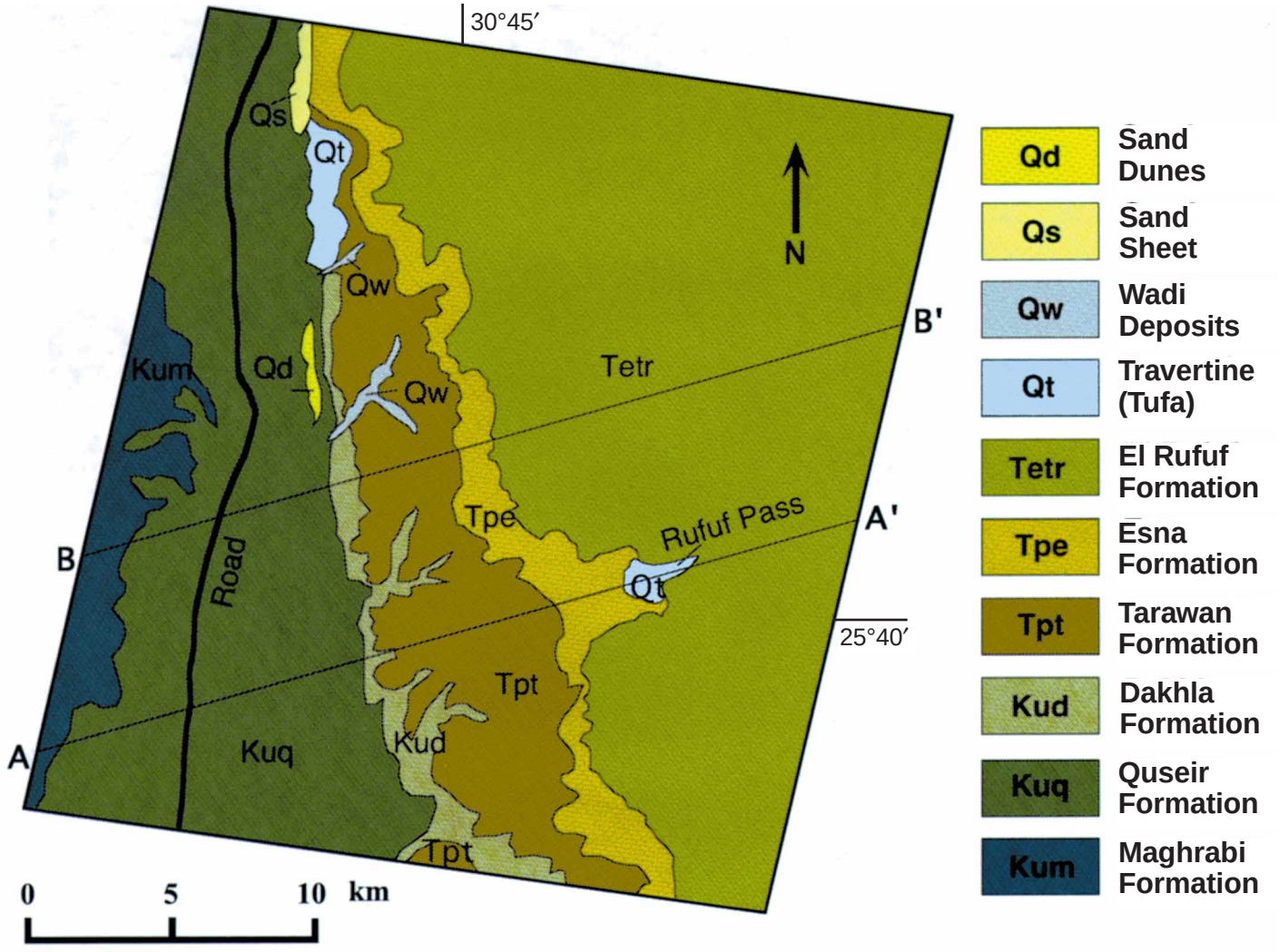

Figure 3. Simplified geologic map of region covered by box a in Figure 1. K = Cretaceous, T = Tertiary and Q = Quaternary. Units are described in text. Cross sections are shown in Figure 4. Units Kum and Kuq floor the Kharga depression, Tpt is located on a plateau 40–50 m above the depression, and Tetr crops out on the main plateau above the depression. Wadi deposits (Qw) map some of the stubby channels. Adapted after Handley et al. (1987).

bands 1 (0.45–0.52 μm in wavelength), 4 (0.76–0.90 μm), and 7 (2.08–2.35 μm) to provide hue and saturation and Système Probatoire d'Observation de la Terre (SPOT) multispectral band 3 (0.79–0.89 μm) to provide intensity. This processing takes advantage of the higher spectral resolution of TM and the higher spatial resolution (20 m) of SPOT. Scalloped edges are evident (Fig. 6, B3, C to D and 4, E5) and individual slump blocks can be identified with a mean width of ≈170 m. Pediments covered with a thin layer of alluvium composed of limestone and shale are on the Esna Formation (shale) between the carbonate units (e.g., Fig. 6, E to F and 4 to 5). A number of alluvial fans can also be identified on the shale units (e.g., Fig. 6, F4-5, I to J and 7). The mixture of limestone and local shale sediments on the fans is consistent with the color patterns (spectral signatures) of the satellite data and is also confirmed by observations in the field.

Comparisons of the color image and geological map illustrate the close correlations between landforms and bedrock geology. Channels superimposed on the Tarawan Formation (Fig. 6, E3-4, G to I and 4 to 6) are wide and have steep walls and flat floors. Channels cut into the El Rufuf Formation on the escarpment and adjacent plateau show similar characteristics (Fig. 6, F to G and 6 to 8). Figure 7 is a map showing the drainage pattern of the study area superimposed with geologic boundaries. This map qualitatively shows that the drainage density is higher in the shale unit (Tpe) than in limestone and chalk units (Tetr and Tpt). The tributaries enter the higher order channels at higher angles in the carbonate units and their lengths are relatively short, forming asymmetric patterns. However, the tributaries in the shale units enter the higher order channels at lower angles and their lengths are relatively long, forming parallel patterns.

The data also suggest a high degree of structural control of sapping landforms. As noted, the major fault systems in the study area are extensional and trend predominantly north-south with deviations to north-northwest and north-northeast and subordinately east-west (Handley et al., 1987; Hermina, 1990). The channels in the Tarawan Formation generally follow these trends. The incipient channels at the high escarpment associated with El Rufuf Pass even more strictly follow the north-south and east-west directions. Figure 8 is a rose diagram of the channel trends in the carbonate units measured from Landsat and SPOT data

Downloaded from gsabulletin.gsapubs.org on December 30, 2009

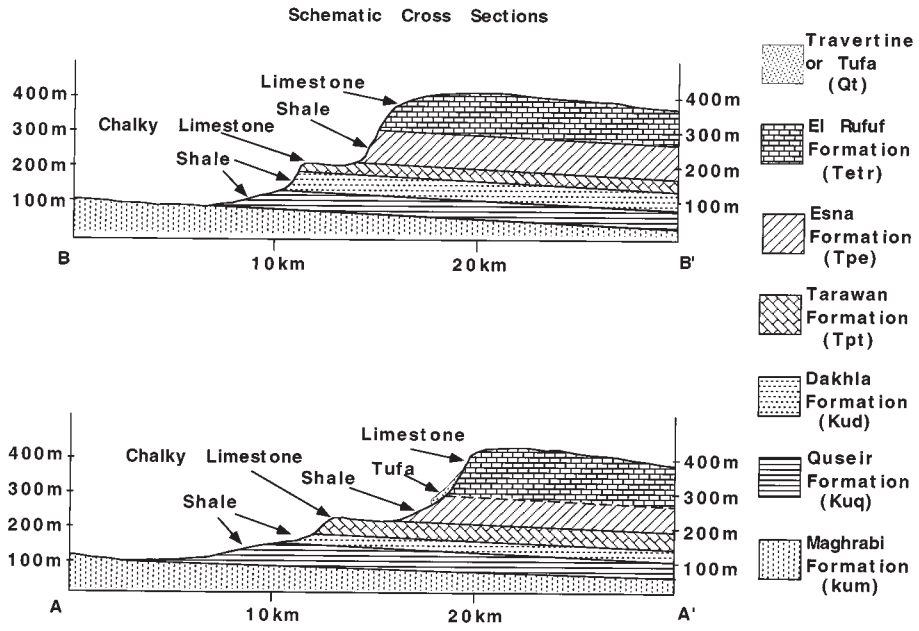

Figure 4. Schematic cross sections along lines AA′ and BB′ in Figure 2. Note the steep escarpment slopes for the limestone (Tetr) and chalky limestone (Tpt) units and the fact that both are underlain by shales (Kud, Tpe). The tufa deposits on limestone bedrock are spring derived. Topographic information from Joint Operations Graphic, 1:250,000, El-Kharga sheet, Defense Mapping Agency Topographic Center (1972).

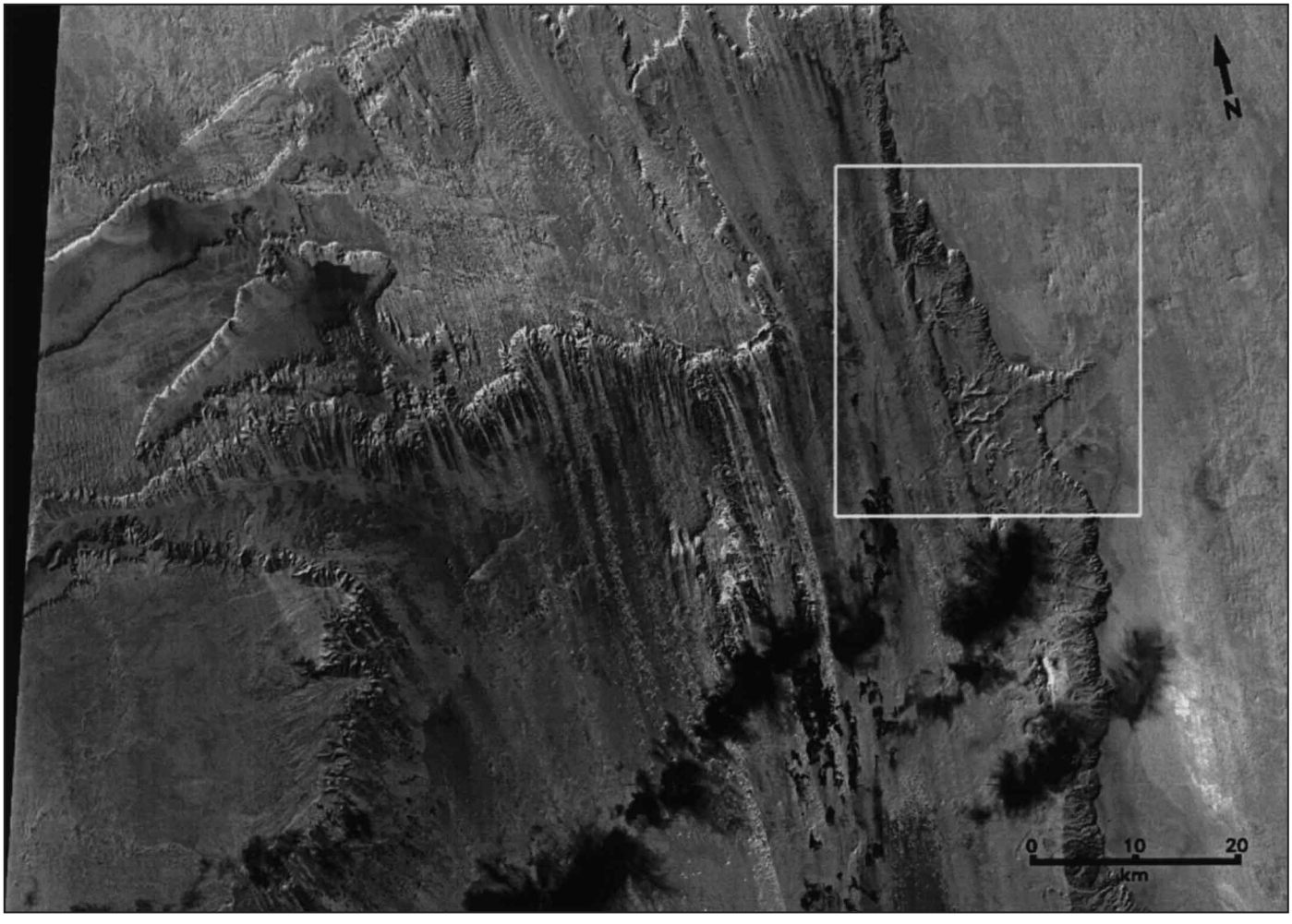

Figure 5. Part of a Landsat Thematic Mapper (TM) scene (band 5) showing a regional view of the northern portion of the Kharga depression. Aeolian streaks extend north-south, indicating dominant wind directions and the current hyperarid conditions. The black patches in the lower half of the scene are clouds and shadows. The box outlines the study area shown in Figures 3 and 6. Note the stubby-looking channels (in Tarawan Formation) and scallop-shaped plateau edges (in El Rufuf Formation) in the boxed area. TM scene product id = TM LS411760428935305. Pixel resolution is 30 m.

Downloaded from gsabulletin.gsapubs.org on December 30, 2009

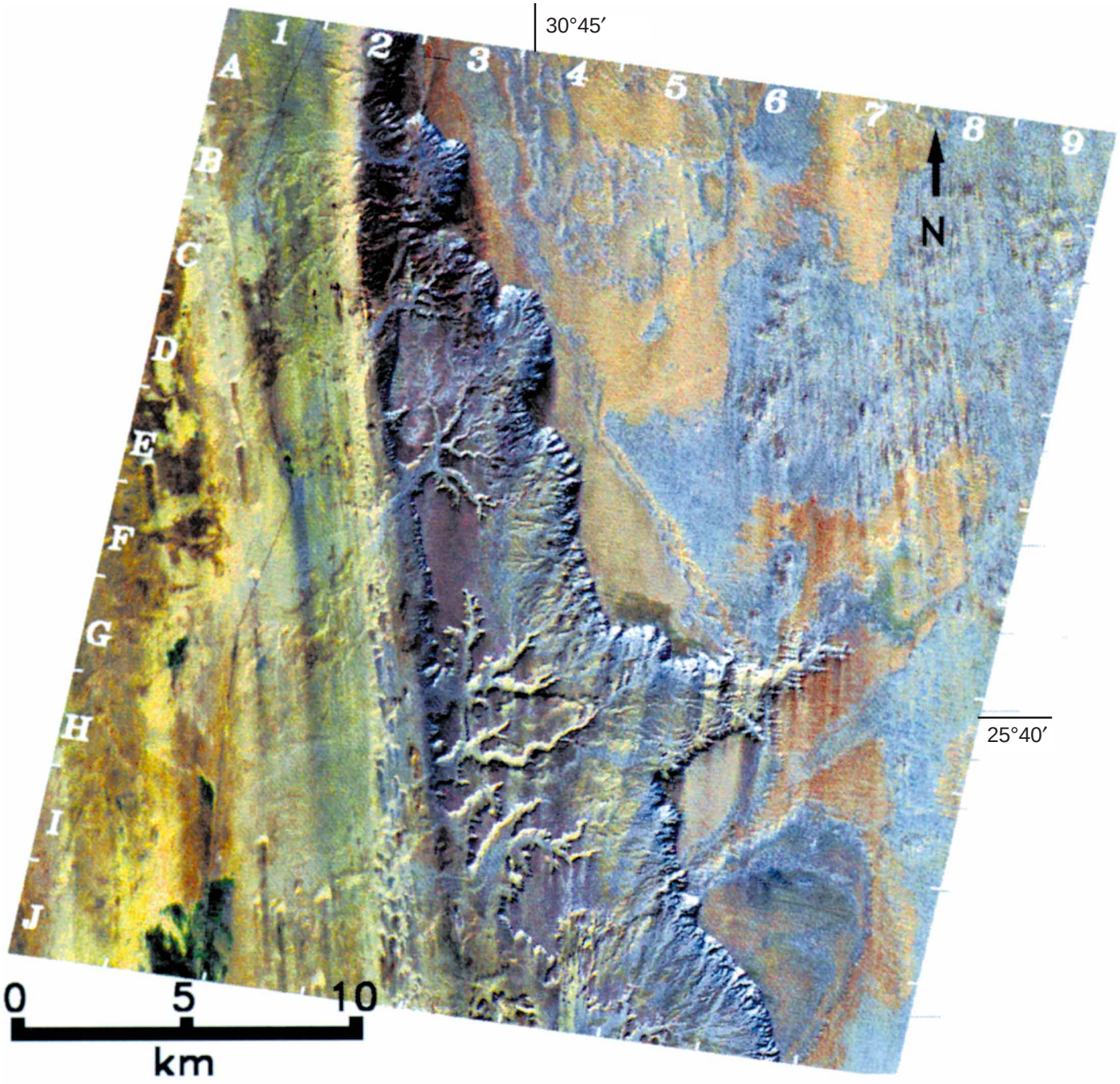

Figure 6. Image of El Rufuf Pass study area constructed by using Thematic Mapper (TM) bands 1, 4, and 7 to provide hue and saturation and SPOT multispectral band 3 to provide intensity, geometrically corrected to compare with geologic map in Figure 2. Sand dunes and wind streaks are visible from coordinates 1–3 and A–J. Areas shown as green (G1-2, J2-3) correspond to vegetation in the Kharga Oasis. Stubby channels are seen in the Tarawan Formation (C3, E3-4, G to I and 4 to 6) and are roughly oriented in north-south, northeast-southwest, east-west directions. Fluvial pediment and alluvial fan systems exist on the Esna Formation to the east of Tarawan Formation (e.g., E to F and 4 to 5, I to J and 7 to 8). The high escarpment is located from A-2 to J-8 and delineates the boundary between the Esna and El Rufuf formations. The escarpment extends into the plateau along a major fault at El Rufuf Pass area (F to G and 7 to 8). Note the scalloped nature of the high escarpment (B3, C to D and 3 to 4). The lack of drainage on the El Rufuf Formation is consistent with high intrinsic permeability associated with karstification. SPOT scene id = (111329819881119083111101X).

Downloaded from gsabulletin.gsapubs.org on December 30, 2009

Figure 7. Drainage patterns of the El Rufuf Pass area superimposed with geologic boundaries. See Figure 3 caption for formation names. Thin lines show the geologic boundaries and the thick lines show the drainage systems. The drainage density in the shale unit (Tpe) is high compared with those in the carbonates units (Tetr and Tpt). The tributaries enter the main streams at high angles in the carbonate units, whereas those in the shale form a parallel pattern. The drainage system is constructed from the satellite data (Fig. 6) using a Geographic Information System software (MGE by Intergraph Corporation).

(Fig. 6), showing that the dominant trends are in north-south, north-east-southwest, and east-west directions. On a regional scale, the locations and the shapes of the depressions also show correlation with structures (Abritton et al., 1990). For example, a north-south–oriented fault passes through the middle of the Kharga depression, and the eastern boundary of the Kharga depression (the big scarp) coincides with a fault (Said, 1962, 1990; Gindy, 1991).

Interpretations. Table 1 is a comparison of characteristics of sapping-dominated and runoff-dominated channels summarized from Hawaii and the Colorado Plateau, two areas where ground-water sapping has been proposed (e.g., Laity and Malin, 1985; Kochel and Piper, 1986; Baker, 1990; Schumm et al., 1995). The channels cut into the El Rufuf Formation (limestone) show all the characteristic planform features caused by ground-water sapping. Moreover, tufa deposits (Fig. 3), in places interbedded with alluvial deposits (Caton-Thompson and Gardner, 1932), provide additional evidence for emergent springs associated with previous epochs of enhanced ground-water. The interbedding of tufa and alluvial deposits indicates that the tufa formation was episodic. Channels cut into the shale units show almost all the features of runoff-dominated channels (Fig. 6 and 7, Table 1). The shift from sapping features on the limestone and chalk units to alluvial features on the shale units is interpreted to be due to a shift in bedrock intrinsic permeability (i.e., from high permeability in carbonates with secondary porosity and high infiltration to low permeability in shales with high runoff). This interpretation is supported by the observation that carbonate rocks exhibit evidence for karstification and thus generation of

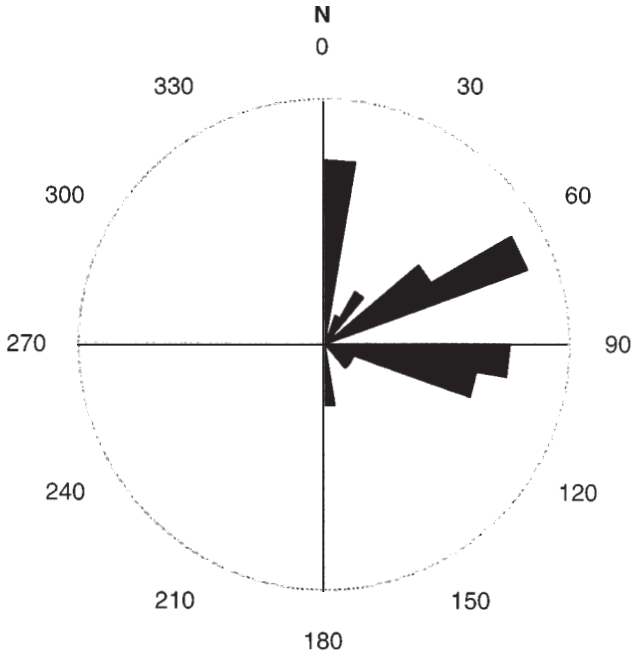

Figure 8. Rose diagram of the trends of channels in the Tarawan Formation and El-Rufuf Formation, measured from SPOT and Thematic Mapper data (i.e., Fig. 6). The major trends are in the north-south, northeast-southwest, and east-west, generally consistent with structural trends of this area documented in the literature (e.g., Hermina, 1990; Said, 1962).

Downloaded from gsabulletin.gsapubs.org on December 30, 2009

TABLE 1. COMPARISON OF GEOMORPHIC CHARACTERISTICS OF SAPPING AND FLUVIAL CHANNELS IN THE COLORADO PLATEAU AND HAWAII

Parameter	Runoff-dominated	Sapping-dominated
Basin shape	Very elongate	Lightbulb shaped
Head termination	Tapered, gradual	Theater, abrupt
Channel trend	Uniform	Variable
Pattern	Parallel	Dendritic
Junction angle	Low (40°–50°)	Higher (55°–65°)
Downstream tributaries	Frequent	Rare
Relief	Low	High
Drainage density	High	Low
Drainage symmetry	Symmetrical	Asymmetrical
Cross-section shape	V-shape	U-shape, steep wall, flat floor
Valley width	Widening downstream	Relatively constant
Tributary length	Relatively long	Short stubby tributary
Structural control	Less strong	Strong
Basin area/canyon area	Very high	Low

Note: Table compiled from Kochel and Pipe (1986) and Schumm et al. (1995).

secondary porosity and permeability in previous wet epochs (Stringfield et al., 1974; El Aref et al., 1987; Said, 1990).

The morphology of the channels in the Tarawan Formation shows features of both runoff-dominated channels (gradual head termination, widening valley downstream, less strong structural control compared with those in the El Rufuf formation) and sapping-dominated channels (e.g., dendritic pattern, high relief, low drainage density, steep wall, and flat floor). These features indicate that they have been inherited from fluvial channels that existed when the Esna shale covered the Tarawan Formation. These features are interpreted to have been modified and widened by ground-water sapping processes as fluvial erosion tapped into the ground-water table (e.g., see Baker, 1988).

The structural control of the orientations of channels in the carbonates units is interpreted to be due to the increased hydraulic conductivities along the fractures associated with the El Rufuf Pass fault system. Sapping landforms developed preferentially along the high hydraulic conductivity zones because of more ground-water discharge along those zones. Figure 9 is a schematic block diagram showing the major geologic and geomorphic features of El Rufuf Pass. Correla-

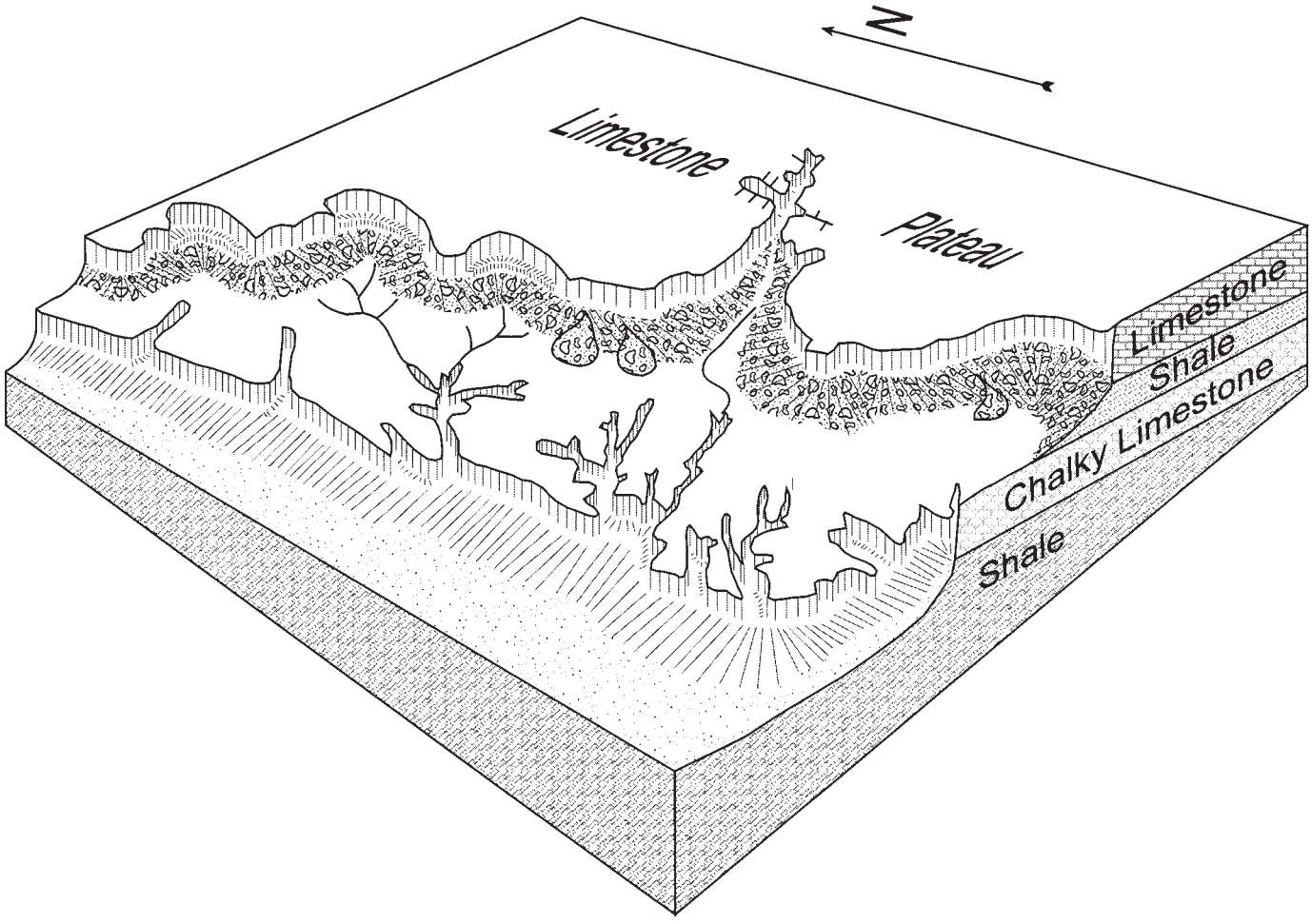

Figure 9. Block diagram of El Rufuf Pass area showing major geomorphic features. A major scalloped escarpment formed in the limestone plateau by differential erosion and ground-water sapping. The slumping blocks developed within the scallops and were disintegrated by weathering and transported downhill by surface runoff. Emerging ground water from the permeable limestone and chalky limestone units formed stubby-looking channels by headward erosion, sapping, and slumping in these units. On the impermeable shale units at the base of the escarpment, surface runoff formed pediments and alluvial fan systems. The lowest shale units formed the depression covered with aeolian sands.

Downloaded from gsabulletin.gsapubs.org on December 30, 2009

tions in location and shape between faults and depressions on a regional scale indicate that the depressions may have been initiated along zones of structural weakness through a combination of processes (Abritton et al., 1990), including fluvial erosion and ground-water sapping.

Farafra Region. *Observations.* Figure 10 is a simplified geologic map of the El Quss Abu Said Plateau study region (area B in Fig. 1). Figure 11 is a SPOT panchromatic image covering part of the Farafra study area. The plateau is about 225 m above the depression floor (Said, 1962). The Khoman Formation, which occupies the eastern part of the depression in Figure 10, consists of white massive neritic chalk and chalky limestone, interfingering with the Dakhla Formation (Hermina, 1990; Klitzsch et al., 1987). The caprock of the oval-shaped plateau consists of the Farafra Formation, which is a member of the Thebes Group and is composed of alveolinid lagoonal limestone (Klitzsch et al., 1987). A sequence of cross-bedded sandstones in a partially kaolinized matrix, known as the Minqar El Talh Formation (Klitzsch et al., 1987), crops out in the southwestern part of the plateau. In the northwestern part of the area shown in Figure 10, the top of the scarp and the plateau surface are composed of Naqb Formation (Thebes Group), which consists of pinkish, dense and nummulitic platform limestones with local flint bands. As in the Kharga study area, the plateau consists of carbonates, and sandstone deposits in the south. The depression is floored by shale-bearing units and chalks. Other units in this area include playa deposits, sand sheets, and sand dunes.

A closer look at the adjacent escarpment reveals a series of arcuate-shaped scallops (Fig. 12, F4, G3), with individual slump blocks inside the scallops. Similar features have also been observed in the Kharga, Kurkur, and Dakhla areas (e.g., Brookes, 1993; Crombie et al., 1995, 1997), where slump blocks slide and rotate downslope, forming a series of steps with tops facing back toward the plateau. The mean widths of these slumping blocks are estimated to be about 150–180 m, on the basis of field observations and measurements from Landsat and SPOT data. Virtually no drainage systems can be identified on the plateau. However, drainage and pediments can be seen adjacent to the base of the escarpment within each scallop. Some alluvial fans develop farther downstream close to the depression (e.g., Fig. 12, I to J and 4 to 5). The southwestern part of the escarpment (Fig. 13) shows more irregular and elongated scallops. In addition, isolated inselbergs are seen in the depression about 1–2 km away from the escarpment. By comparing the geologic map and SPOT data, it is clear that well-developed scallops formed in limestones (Fig. 12), whereas more irregularly shaped and elongated scallops developed in sandstones (Fig. 13).

Interpretation. Arcuate-shaped scallops are typically formed by rock failure and downslope slumping (e.g., Selby, 1993, p. 258–260). The scallops formed this way usually have the shape of an amphitheater, an arcuate shape not only in plan view, but also in profile view. Studying similar features in the Dahkla area, Brookes (1993) attribute the formation of the scallops to ground-water saturation and deconsolidation of the underlying shale, which leads to slides of the overlying limestones, forming arcuate-shaped scallops. Issar (1982) also concluded that basal ground-water seepage is usually a major triggering factor for the slides that form the scallops (or erosion cirques) observed in the Sinai and Negev. In the Farafra area, the source water for the drainage systems emanating from these scallops must have been ground-water from the carbonates on the plateau. This interpretation is consistent with the lack of upslope catchments and feeder channels on the plateau, implying rapid infiltration of surface water into the subsurface of the limestone plateau. The differences in morphology at the escarpment edges between limestone and sandstone caprocks indicate control by bedrock type. The more resistant sandstone may be less susceptible to sapping mobilization than limestone. The observations also suggest that surface runoff has been minimized on the plateau due to infiltration into the subsurface. Ground-water seeped out at the scarp face, causing weakening of the shales and mass wasting of overlying material, followed by retreat of the escarpment and formation of the arcuate-shaped scallops at the plateau edge. The emergent ground-water, coupled with local rainfall and runoff, formed the fan systems consisting of a mixture of sandstone and local shales. Similar patterns are evident in the Kharga and the Kurkur areas.

Tufa Ages

To understand the timing of the ground-water sapping processes better, a number of tufa samples were collected from Kharga, Farafra, and Kurkur areas and dated using uranium-series disequilibrium methods (Sultan et al., 1996; Crombie et al., 1995, 1997). Crombie et al. (1995, 1997) examined the samples petrographically and point counted for micrite, sparite, and pore space. Samples with less than ≈75% micrite contained obvious recrystallization and secondary recrystallization features. Samples with greater than 75% micrite were homogeneous with no obvious secondary alteration. The ages of samples with greater than 75% micrite are therefore more reliable than those with lower micrite contents. These data cluster around 100 and 200 ka, correlating with the major interglacial marine oxygen isotope stages (Crombie et al., 1995, 1997). These data, along with those of Szabo et al. (1995), suggest that tufa-forming pluvial episodes coincide with major intergalcial periods.

CONCEPTUAL MODEL

On the basis of the observations described above and the climatic history of the area in the literature, a qualitative conceptual model for the landform development can be constructed (Fig. 2). Egypt is thought to have had a much wetter climate throughout most of the Tertiary Period (Said, 1990) and to have become progressively colder and drier since the Pliocene Period (3.2 Ma, Said, 1990) to late Pleistocene Period (1.8 Ma, Van Zinderen Bakker and Mercer, 1986). The change is thought to be due to the changes in atmospheric circulation patterns in northeastern Africa (Prell and Kutzbach, 1987). Under humid climatic conditions, karst dissolution and fluvial erosion would have been the dominant geomorphic processes, forming the karst features such as caves, karren, rainpits, and sinkholes commonly found in the limestone country of the mid-latitude Egypt (Stringfield et al., 1974; El Aref et al., 1987; Haynes, 1982). The karstic cavities with terra rosa soil fillings in the plateau limestones (Haynes, 1982) are likely to have formed during these humid periods. As the system changed from humid to arid, fluvial erosion (rather than karstification) would have begun to dominate, including differential erosion to produce the escarpments between shale-floored depressions and limestone plateaus (McCauley et al., 1982; Albritton et al., 1990). The initiation of depressions is likely to have happened at the structurally weak zones such as fault lines.

The characteristic requirements for ground-water sapping are met by a permeable limestone aquifer with increased permeability formed during karstification processes, a ground-water system recharged by local rainfall and regional ground-water flow, a free surface formed by differential erosion, structural and lithologic inhomogeneity, and fluvial processes to transport material released from the scarp face. As the climate became more arid, ground-water seeping from the initial escarpment, the associated saturation and deconsolidation of the shale units, subsequent breakup and slumping of the overlying limestone units, and removal of broken materials by surface runoff would have become the major processes responsible for the enhancement and retreat of escarpments. As the climate transformed to the cur-

Downloaded from gsabulletin.gsapubs.org on December 30, 2009

rent hyperarid conditions, escarpment retreat would have slowed and aeolian processes would have become dominant, forming the sand dunes and wind streaks found in the region.

NUMERICAL MODEL FOR ESCARPMENT GENERATION AND EVOLUTION

With a conceptual model for development of depressions, escarpments, and associated features, the next step was to provide a predictive, quantitative model that simulates the processes and features (Fig. 2). The model should not be viewed as a detailed simulation of every aspect of the processes and resultant landforms and deposits. For example, the model does not include karstification. We assume that karstification and associated permeability and porosity developed in earlier periods (most of the Tertiary), when northeastern Africa was more humid (e.g., Said, 1990; Van Zinderen Bakker and Mercer, 1986). Tectonic activity is also ignored because the Western Desert was tectonically quiescent during the time period of interest (Gindy, 1991). The model concentrates on simulating first-order processes associated with fluvial erosion and ground-water sapping under semiarid to arid climatic conditions since the beginning of the Pleistocene. The purposes of the simulations are to gain insights into the interactions and coupling between hydrology and geomorphology systems and their effects on landform evolution, to test the importance of structural control, and to show the extent to which resultant landforms and deposits maintain evidence of past climatic changes.

In the model, fluvial processes are based on the cellular automata technique (Chase, 1992). This technique merges the detailed small-scale geomorphic processes into a few parameters and a set of simple rules that are iteratively applied to individual cells of a topographic grid. This approach is similar to studying heat transport or mechanics in physics by dealing with large-scale laws rather than worrying about the motions of individual particles (Chase, 1992). The stochastic element is introduced in the model by randomly dropping rainfall events (termed "precipitons") onto the topographic grid. The precipiton activities are then determined by the rules and the parameters of the cell where that precipiton resides and its neighbors.

The ground-water sapping part of the model follows the work of Howard (1988), with an extension to transient flow conditions. The model is based on the assumption that ground-water sapping occurs where a critical specific discharge rate (volume flux per unit area) is exceeded (Howard, 1988, 1994). This is a reasonable assumption because the seepage force, which is a body force acting on some representative volume of the porous medium by fluid drag (or shear) to reduce its internal resistance to rupture (e.g., Dunne, 1990), is proportional to the specific discharge of ground-water flowing through the volume (e.g., Bear, 1972, p. 184–186; Iverson and Major, 1986). The seepage force is responsible for the entrainment of soil or rock and causes subsequent upslope failure. Howard (1988) used this assumption in his model and produced landforms consistent with those from physical sandbox experiment. The second assumption is that the ground-water flow can be approximated by an unconfined aquifer with the Dupuit assumption (ignoring the vertical component of flow, Howard, 1988). Considering the gentle dip of the limestone formations in the Western Desert of Egypt and the lack of tectonic activity in this area, this assumption is justified. The water table is calculated using an implicit finite difference iteration method (Wang and Anderson, 1982) at each time step after the topography and recharge change. The amount of erosion when sapping is initiated is proportional to the discharge rate over the critical value and to the erodibility of the material. The discharge rate is calculated using Darcy's law. Erosion and deposition by ground-water sapping are incorporated into the cellular automata scheme. The slumping associated with ground-water sapping can be modeled by cell-based diffusion if the cell size is set to the characteristic width of the slumping block. The slumping (cell-based diffusion) is determined by local surface slope.

The details of the modeling and the program codes were documented in Luo (1995). Figure 14 is a schematic flow diagram of the computer simulation. The simulation starts with an initial topographic grid and ground-water table. If a storm occurs over a grid site, precipitation, diffusion, infiltration, fluvial erosion, and deposition modules are executed. Sapping routines are executed if the conditions for ground-water sapping erosion are satisfied, i.e., the discharge rate exceeds some critical value (Howard, 1988). The diffusion routine, which simulates mass wasting and soil creep (Chase, 1992), is also executed when sapping occurs. The diffusion mimics sapping failure because we selected the cell widths based on field observations of slump blocks. To simulate the contribution from regional ground-water flow, a regional recharge term is uniformly applied from the top to the model, because the regional flow does not change much spatially over the study area (Brinkmann et al., 1987). The ground-water table is then recalculated. The simulation advances into the next time step and the above procedures are repeated until the end of the simulation. Rainfall, storm frequency, and regional recharge can be varied over time, simulating climatic change.

Rainfall events (called precipitons) are modeled with a Poisson magnitude distribution for precipitation and the surface flow velocity used in erosion is calculated using the Chezy equation. The cellular automata algorithm of fluvial processes works as follows (1) A storm of some parameterized Poisson magnitude distribution (to match mean annual rainfall) is dropped randomly onto a cell of the topographic grid with water moving to the lowest of the eight neighboring cells. (2) As water moves downhill, it infiltrates into the subsurface, based on an empirical method of the U.S. Soil Conservation Service (Bras, 1990). (3) At the same time, erosion occurs if the parameterized carrying capacity of the storm is not exceeded. Erosion is proportional to the surface flow velocity (calculated by the Chezy equation) and to the erodibility of the material (bedrock and sediment have different erodibility). (4) If the carrying capacity is exceeded, deposition occurs. (5) The diffusion routine is executed when each precipiton first drops onto the topographic grid. Linear Fickean diffusion is assumed and is carried out by downhill transport between the target cell and its four nearest neighbors. The material diffuses onto the neighbor cell if that neighbor cell is lower than the target cell. The direction of diffusion is opposite if the neighbor cell is higher than the target cell. The amount of diffusion is proportional to local slope and is inversely proportional to the square of the cell size (Chase, 1992).

The interactions between surface and subsurface processes are conducted as follows. Surface water infiltrates and feeds ground-water as recharge, the amount that infiltrates being subtracted from the surface flow. Ground-water that intersects the land surface flows downhill as surface overland flow using surface erosion and deposition routines. This event is called a sappaton (in contrast to precipiton, a rainfall event). The water table is then lowered by applying negative recharge for the part becoming overland flow.

The generation of spring-derived tufa deposits can be described by the following reaction:

$$\begin{array}{c} CO_2(g) \\ \Updownarrow \\ H_2O + CaCO_3 + CO_2(aq) \Leftrightarrow Ca^{2+} + 2HCO_3^-. \end{array}$$

CO_2 is released into the atmosphere (CO_2[g]) as the water emerges from the ground, driving the reaction toward the left. In other words, the ground-water undersaturated with respect to $CaCO_3$ becomes oversaturated as CO_2 is released. This process is modeled in a parametric way by having a tufa deposition rate proportional to the spring discharge rate. Once deposited, the tufas are subject to fluvial and sapping erosion. The model keeps track of the

Downloaded from gsabulletin.gsapubs.org on December 30, 2009

times when tufas are first deposited or completely eroded away (because keeping track of all the deposition and erosion events is impractical). This information is used herein to calculate the oldest age of the tufas preserved in each cell. The calculated model tufa ages are then compared with actual U/Th ages of tufa samples acquired in Kharga, Farafra, and Kurkur by us as part of our ongoing research (e.g., Sultan et al., 1996; Crombie et al., 1995, 1997) to explore the extent to which landforms and deposits carry evidence of past climatic changes.

The model has two rock layers, i.e., a resistant but permeable top layer simulating limestones (or sandstones) and an erodible but impermeable bottom layer simulating shales (Fig. 15). The top layer will be referred to as limestone and the bottom layer as shale. For simplicity, both layers are assumed to be horizontal (Fig. 15). Because the deep Nubian aquifer (beneath the shales) is not included in this two-layer model, possible contributions to recharge by upward leakage from the Nubian aquifer are only implicitly included in the regional recharge term, which is applied uniformly from the top to the model. Explicit treatment of upward leakage from the Nubian aquifer would require a multilayer model, which would considerably increase the complexity of the model and is beyond the scope of this paper. The present two-layer treatment suffices to simulate the first-order features, because the emergent ground-water would have the same sapping effects on geomorphology, regardless of its source.

The boundary conditions for the ground-water flow within the permeable limestone layer are no flow through the boundaries parallel to the long sides, no flow through the boundary with the highest elevation, and constant head at the side that coincides with the outcrop of the limestone-shale boundary (Fig. 15). The no-flow boundary condition at the boundary with highest elevation simulates the ground-water divide. Because the local hydraulic gradient is from the plateau toward the depression, the no-flow boundary conditions at the boundaries parallel to the long sides are reasonable. The constant head is taken as the height of the bottom of the limestone layer, because that is the lowest head under the assumption that the underlying shale is impermeable. This set of boundary conditions also mimics a physical sandbox model with one side open (Howard, 1988).

MODEL PARAMETER ESTIMATION

The next step in model development was to select appropriate values for each parameter so that the model produced realistic results (Fig. 2). The parameters involve paleogeomorphology, paleoclimate, paleohydrology, lithology, and structure. Wherever possible, we selected parameter values based on independent measurements (direct or indirect) documented in the literature. For the parameters that lacked independent measurements, model results were used to determine the most probable values, based on comparisons of model landforms, generated using different values, with actual observations. The parameters, their values, and categories are listed in Table 2 and are grouped by the ways that their values were determined, i.e., whether the values were independently known, or solved using the model.

Independently Known Parameters

The critical discharge rate represents the susceptibility of the bedrock to ground-water sapping failure. Many landslide and slope-failure studies measure the critical conditions for failure in terms of rainfall duration and intensity (e.g., Caine, 1980; Larsen and Simon, 1993). However, the timing, duration, and speed of slide movement do not always correlate directly with the timing and amount of rainfall (Iverson and Major, 1987). Iverson and Major (1987) conducted detailed measurements of ground-water conditions in the Minor Creek landslides, northwestern California, and found that the ground-water hydraulic gradient is the factor most responsible for failure. On the basis of their detailed head measurements, they found that the mean hydraulic gradient that triggers seasonal motion at Minor Creek landslide corresponds well with typical wet-season hydraulic gradient, which was estimated as 0.6–0.7 (Iverson and Major, 1987). Their hydraulic conductivities based on slug tests were approximately log-normally distributed and the representative value (geometric mean) is 5×10^{-8} m/s, which will give a critical discharge rate estimate of about ≈0.002 m/day, according to Darcy's law. Due to the lack of other measurements and the difficulty of dealing with a paleohydrology system, this value was used in our model.

The model simulates slumping by cell-based diffusion. Thus, the cell size selected must reflect the characteristic size of the slumping blocks observed in the field. On the basis of field observations in Kharga, Farafra, and Kurkur areas, and measurements on Landsat and SPOT data, a size of 170 m was selected.

The only direct hydraulic conductivity measurements in the study area are for the deep Nubian sandstone aquifer (e.g., Hesse et al., 1987). Hydraulic conductivities for limestones are variable, ranging from 0.00008 m/day for crystalline rocks to 0.5 m/day for rocks with secondary permeability through fracturing or dissolution (Domenico and Schwartz, 1990). On the basis of the fact that there are secondary porosities from karstification under earlier humid conditions in the study area, the hydraulic conductivities for limestones in the model were assumed to be 0.1 m/day. The storage coefficient, which represents the volume of water released from storage per unit area of aquifer per unit decline in head, was taken to be 0.2, within the range of unconfined sandstone and limestone aquifers (Domenico and Schwartz, 1990).

Linear zones of high hydraulic conductivity and erodibility were introduced at ≈5° from the grid directions (assuming north-south, east-west) to simulate the control of fractures on erosional features (Fig. 15). This orientation of fractures was selected because the major fault directions in the study area were primarily along, but slightly off, the north-south, east-west directions (Fig. 6 and 8). The fractures can be turned on or off for comparison.

To model the climatic change of the area, a composite deep-sea core $\delta^{18}O$ record (Prell and Kutzbach, 1987; Clemens et al., 1991; Imbrie et al., 1993) was used to scale the mean rainfall history. The following reasons justify the use of the $\delta^{18}O$ record as the first-order estimate of climate conditions of the study area. The deep-sea core $\delta^{18}O$ record is known to be controlled by global ice volume and sea-surface temperature (e.g., Dawson, 1992). High values correspond to glacial epochs, whereas low values correspond to interglacial epochs. This record is directly related to Northern Hemisphere summer insolation and is a proxy for overall climatic conditions in northeastern Africa (Imbrie and Imbrie, 1980; Prell and Kutzbach, 1987; Clemens et al., 1991). High solar insolation is thought to intensify summer monsoonal activity, moving the Sahel wetting front into northeastern Africa (Nicholson and Folhn, 1980; Rossignol-Strick, 1985; Haynes, 1987; Prell and Kutzbach, 1987). U/Th and radiocarbon dating of lacustrine deposits of southern Egypt and northern Sudan by Szabo et al. (1995) correlate well with the major interglacial marine oxygen isotope stages. Faunal assemblages of the same general area also point to northward displacement of the monsoon belt during interglacial times (Kowalski et al., 1989). Furthermore, the $\delta^{18}O$ record matches the lake-level data of Street-Perrott and Harrison (1984). The advantage of using the $\delta^{18}O$ record over lake-level data is that the $\delta^{18}O$ record extends over millions of years, whereas the lake data only go back to 140 ka.

The present mean annual rainfall was taken and the values for the past were scaled using a smoothed version of the deep-sea core $\delta^{18}O$ record (Fig. 16). A smoothed version of the $\delta^{18}O$ record was used to scale rainfall because the U/Th dating of tufa samples suggests that tufas only form during major pluvial times (Szabo et al., 1995; Crombie et al., 1995, 1997). The indi-

Downloaded from gsabulletin.gsapubs.org on December 30, 2009

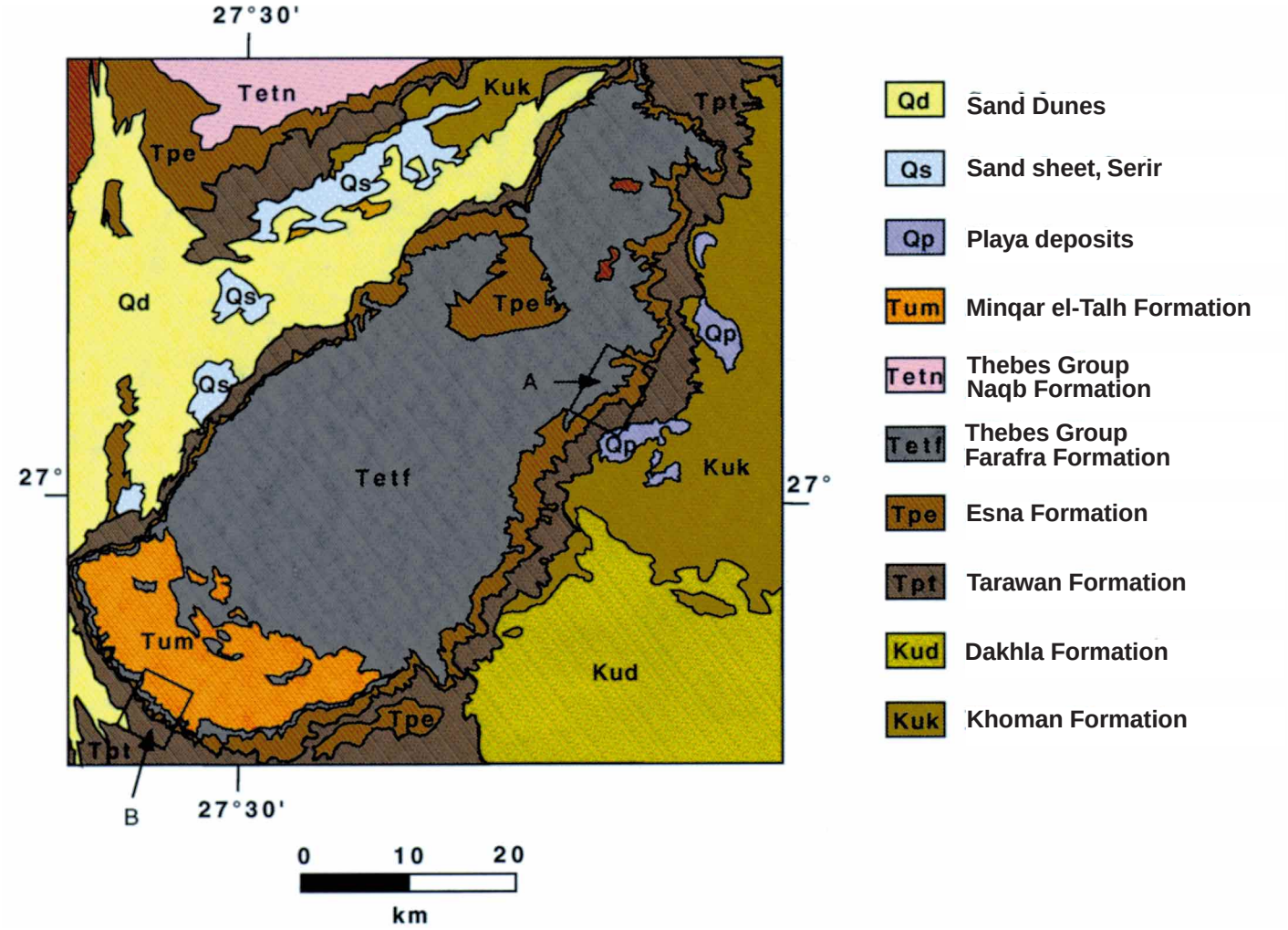

Figure 10. Simplified geologic map of Quss Abu Said Plateau, Farafra. K = Cretaceous, T = Tertiary, Q = Quaternary. Units are described in text. Details of areas A and B are shown in Figures 12 and 13, respectively. Adapted after Klitzsch et al. (1987).

vidual peaks are not as important as the general trend. The smoothed version also shows the general drying trend more clearly (Fig. 16). Furthermore, with this scaling, the average rainfall two million years ago is similar to the present value at the southern Sahel wetting front (Thompson, 1965), consistent with the supposedly northward movement of this wetting front in the past. The regional recharge and storm interval (inverse of frequency) were also varied according to the rainfall history. The regional recharge was set to be proportional to the rainfall function. The interval between storms was scaled according to the rainfall function so that there are more rainfall events (short intervals) during wet periods and fewer events during dry periods.

Model-Derived Parameters

The erodibility is a dimensionless parameter. The relative values of erodibility reflect the differences in lithology and the absolute values set the time scale of the model and the denudation rates. The shale erodibility listed in Table 2 was selected by running the model and comparing the resultant denudation rates with continental denudation rates (2–50 mm/k.y.) independently estimated from the mechanical and chemical load of catchment rivers (e.g., Gilchrist and Summerfield, 1992; Berner and Berner, 1987; Thomas, 1994; Pavich, 1985). The erodibility of the limestones was assigned to be two orders of magnitude lower than that of the shales (Table 2), because this difference was needed to produce escarpment relief consistent with observations. Tufa and limestone are both observed in the field to be more resistant than shales, so they were assigned the same erodibilities. Material eroded from the bedrock was regarded as unconsolidated sediment and had an erodibility two times higher than that of shales. This value was selected on the basis of comparison of actual and modeled depositional patterns. Higher values resulted in little sediment deposition and alluvial fan accumulation.

The sapping erosion scaling factor is the proportionality constant for calculating the amount of sapping erosion (Howard, 1988). The value listed in Table 2 was determined by comparison of model runs with observations. The criteria were that the overall resultant model morphology should look similar to the observations (i.e., with an escarpment and scallops in the limestone and alluvial fans and pediments in the shale) and there should be no unrealistic singular points (deep holes or high spikes) in the resultant model topography. The product of the scaling factor and the discharge needed to be small enough so as not to make deep holes in the limestones. Model runs with different values (10 at the low end and 100 at the high end) for the sapping scaling fac-

Downloaded from gsabulletin.gsapubs.org on December 30, 2009

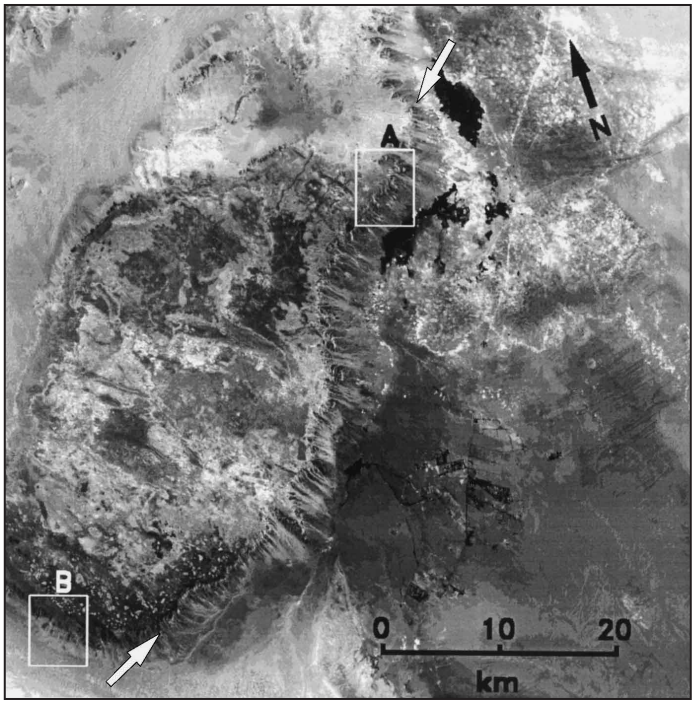

Figure 11. SPOT panchromatic image covering the Farafra study area. The oval-shaped body in the western portion of the image is El Quss Abu Said Plateau. The plateau is composed of mostly limestone of Farafra Formation. The areas with dark albedo in the southwestern corner of the plateau are sandstones of Mingqar El-Talh Formation. White arrows delineate the eastern escarpment, along which a series of pediments and alluvial fans can be identified. Details of areas A and B are shown in Figures 12 and 13, respectively. To the east of the escarpment is the Farafra depression. The black patches in the northeastern part of the scene are playa deposits. SPOT scene id = (110629619930709090834O1P)

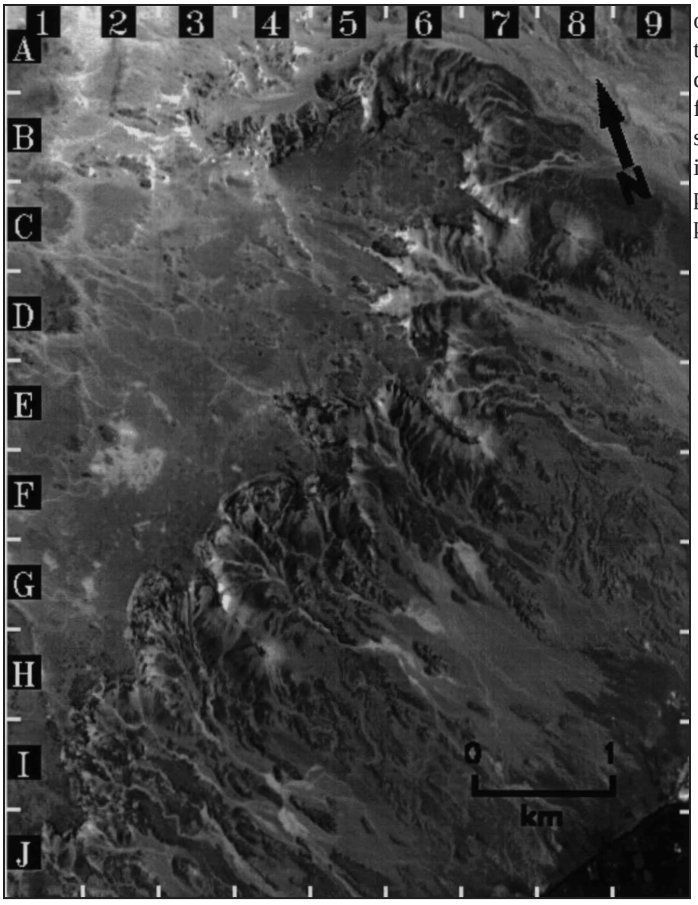

Figure 12. Enlargement of box A in Figure 11. The escarpment extends from coordinates J-1 to B-7. To the west of this line is the limestone plateau and to the east is the depression underlain by Dakhla Formation (shales) and Khoman Formation (chalks). No drainage system is evident on the plateau, but there are channels emanating from the base of the escarpment and draining into the depression. The scallop-shaped features along the edge of the escarpment are located at coordinates F to G and 3 to 4. Also note the linear ridges trending northwest-southeast between adjacent scallops (H to G and 3 to 4, E6-7).

tor did not result in significantly different landforms. However, the retreat rates of the escarpment were different. An erosion scaling factor value of 50 generated escarpment retreat rates similar to a rough estimate based on tufas on the outliers several hundred meters in front of the escarpment (see model results). Thus, the value of 50 is a reasonable estimate for this parameter.

The scaling factor (proportional constant) for tufa generation listed in Table 2 was set so that the deposition of tufa was distributed close to the escarpment and did not generate topographic spikes. Tests with the tufa generation scaling factor showed that models with a higher value (e.g., 0.1) would generate excessive tufa buildups in front of the escarpment, which would impede the escarpment generation and retreat. With the value listed in Table 2, the model produced tufa thicknesses within the range of observation (2–10 m, Crombie, 1996). Thus, this value seems reasonable.

The initial topography was represented by a 100×200 grid with elevation at each point covering an area of about 17 km by 34 km (Fig. 15). The grid size was chosen as a compromise between the computation time and edge effects. A larger grid size takes more time to run and a smaller size will have edge effects. The model with a smaller grid size of 50×100 took less computer time and produced scalloped escarpments with sizes and shapes similar to those produced by the model with a grid size of 100×200. The grid size did not seem to affect the planform morphology. However, in the 50×100 model, headward and sideways erosion quickly reached the edges of the modeling domain and resulted in unrealistic excessive downward erosion. With a grid size of 100×200, the model usually takes about 2.5 days to finish 2 m.y. of simulation on a Silicon Graphics Challenge system, without causing any edge effects. Grid sizes larger than 100×200 also produced similar planform morphology with no edge effects, but they take weeks. Thus, a size of 100×200 is reasonable for the simulations.

The initial topography two million years ago is unknown. A simple peneplain was selected as a convenient initial topography for the modeling. The slope of the peneplain is set to be very gentle (1%) because the plateau surface has very gentle regional tilt toward the depressions (≈1%, Defense mapping Agency Topographic Center, 1972) and the area is thought to have been tectonically quiescent (Gindy, 1991). Model runs with an initial topographic slope greater than 10% resulted in smooth topography and larger spacings between channels, because the amount of the diffusion is pro-por-

Downloaded from gsabulletin.gsapubs.org on December 30, 2009

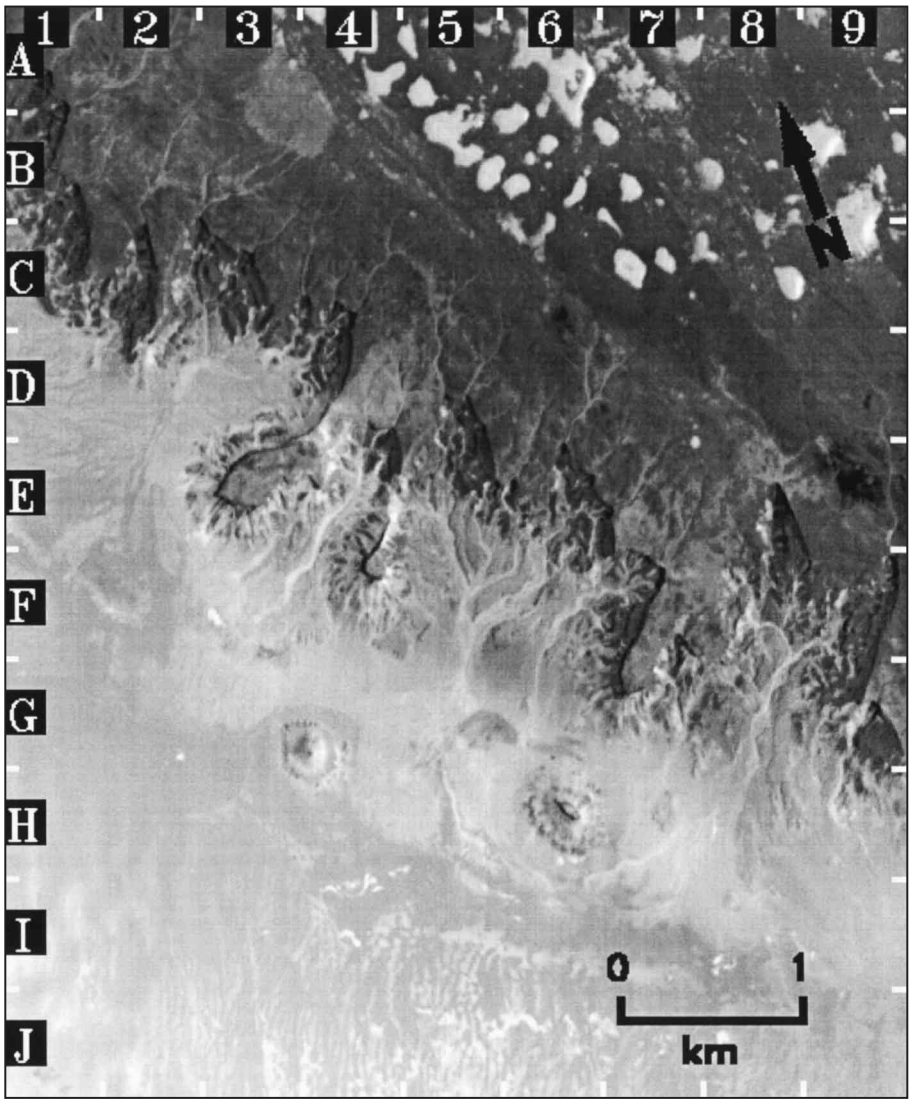

Figure 13. Enlargement of box B in Figure 11. The escarpment extends from B1 to G9. To the north of the escarpment is the plateau, composed of sandstone of the Minqar El-Talh Formation. To the south is the depression underlain by the Esna (shales) and Tarawan formations (chalks). The scallops along the escarpment (E to F and 3 to 4, E to G and 7) are more elongated and more irregular compared to those shown in Figure 10. The ridges between the scallops are also wider and isolated inselbergs are left in the depression (G to H and 3 to 4, H6).

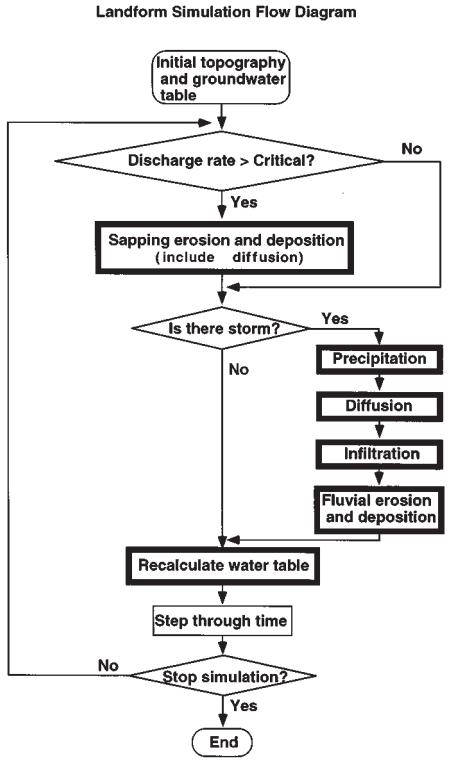

Figure 14. Flow diagram of the computer simulation illustrating erosion, deposition, and ground-water sapping processes and their interactions. See text for details.

tional to slope. An initial topography with an existing escarpment was also attempted. The result was not significantly different from that with a gently tilted peneplain because for a tilted peneplain, differential erosion between limestone and shale quickly developed an escarpment. In other words, a dynamic equilibrium is established after the model started. Thus, the initial topography does not seem to affect the final landform and a simple gently tilted peneplain is a reasonable starting condition.

Hydraulic conductivities in fractures should be higher than the surroundings. However, there are no data that we are aware of in the study area about how high conductivities would be. In the model, the hydraulic conductivities were increased by a factor of two over that of the limestone, because model runs with higher values caused the water table to drop rapidly, and few tufas were formed and none preserved.

Discussion

To summarize, most of the key model parameters were estimated based on some independent measurements (Table 2). The rest, most of which are dimensionless parameters, were determined based on the model by comparing the model results with the observed landform, sediment distribution, and thickness (Table 2). One may argue that the second method of determining the parameters is self-serving and that the modeling is circular reasoning. To address this concern, we conducted numerous model runs in which we varied these parameters one at a time to determine their control on model results. Tests indicate that initial topography does not affect the final landform as dynamic equilibrium is achieved. Furthermore, we have used a grid size that did not result in any edge effects. In addition, the tufa generation scaling factor produced tufa thicknesses within the range of observations and the sapping scaling factor generated scarp retreat rates consistent with rough estimates from observations. Thus, these model-determined parameters are reasonable. The estimation of erodibilities was model derived, but was also based on independently measured continental denudation rates. The model results based on these values should be predictive and the model should at least provide some insights into the long-term evolution of surface and subsurface processes under a changing climate.

Downloaded from gsabulletin.gsapubs.org on December 30, 2009

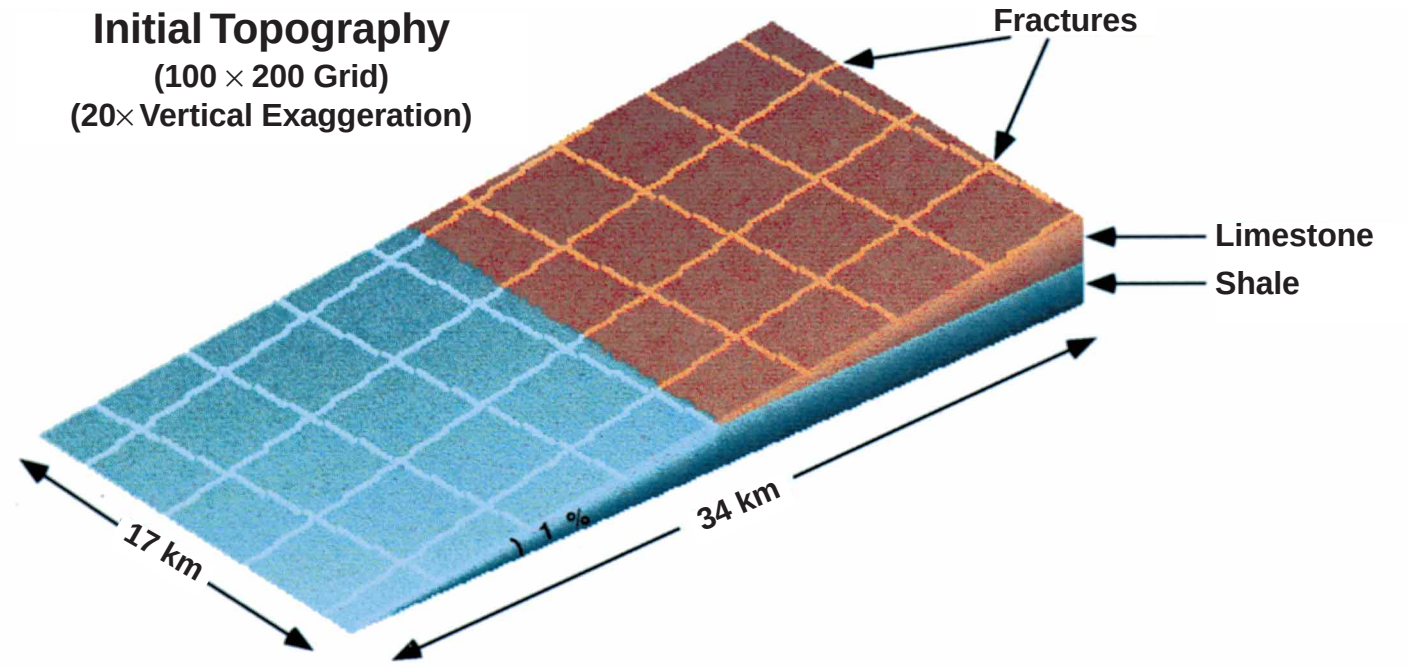

Figure 15. Initial topography and stratigraphy. The slope of the topography surface is 1% (thus Dupuit assumption is valid). The pink is limestone and the bluish-green is shale. Bright lines are high hydraulic conductivity and erodibility zones to simulate fractures (in the shale layer, the bright zones only represent high erodibility). The two layers are assumed to be horizontal. Ground-water flow only operates in the limestone layer.

MODEL RESULTS

With a reasonable set of parameter values determined, in this section we discuss the model results and the insights the predictive model can provide (Fig. 2). Two cases, with and without simulated fracture zones, are presented. For the case with no fractures (Fig. 20a), an initial escarpment formed at the outcrop of the boundary between the limestone and shale due to differential erosion. This initial scarp face is essential for ground-water sapping processes to be initiated because it provided a free surface for ground-water to seep out easily. The initial escarpment was then enhanced and retreated by ground-water sapping and slumping processes. Thus, it is differential erosion that initiated ground-water sapping and slumping processes, and caused the landform evolution. In addition, scallops and linear ridges between adjacent scallops formed in the limestones. Pediments and alluvial fans formed on the shale units. Tufas were deposited where the ground-water intercepted the surfaces (Fig. 20a). They were also removed by fluvial erosion processes. The ground-water table dropped with time as the climate became dry. Some older tufas were preserved on the plateau between scallops (Fig. 20a). The model kept track of the amount of erosion, and thus vertical erosion and horizontal retreat as a function of time and their rates (slope) can be inferred (Fig. 17). The vertical erosion rate and scarp retreat rate declined with time. The scarp retreat decreased from several kilometers in the first million years to several hundred meters during the most recent million years. The tufas on scarp outliers northwest of Kharga are thought to be mid-Pleistocene, and they are only a few hundred meters in front of the scarp, implying that headward erosion accounts for several hundred meters per million years (Maxwell, 1995, personal commun.). The model-predicted values are consistent with this interpretation.

The models also provided insight into the details of ground-water sapping processes. The fluvial erosion not only created a scarp face at the surface boundary between shale and limestone, but also generated local depressions in the limestone along the scarp face. Because precipitons are not uniformly but randomly dropped onto the topographic surface, some points along the initial scarp face will be eroded before others, even if they have the same erodibility. This creates small local depressions. The ground-water table, which was very close to the surface at the initial scarp face, became depressed at those local depressions, because the water table followed topography (Fig. 18a). The depressed water table led to concentration of ground-water flow lines toward the local depressions and an increase in discharge due to higher water-table gradients (Fig. 18a). Sapping events (sappatons) were initiated at those places where ground-water flow exceeded the critical discharge value for ground-water sapping. Sapping erosion, i.e., associated slumping and removal of materials out of the sapping site by fluvial transport, further depressed the topography and ground-water table, causing even more erosion. This positive feedback mechanism continued to favor erosion at those initial local depressions and the initial scarp face, which eventually formed scallops and a retreating escarpment (Fig. 20a). Thus, fluvial process and ground-water sapping working together generated the landform and deposits. Without fluvial processes, there would be no continued scarp retreat.

Examination of the model landforms at short time intervals shows that the sappatons initially created the lightbulb-shaped scallops that were subsequently expanded upslope and laterally. Similar phenomena have been observed in modern humid environments in Madagascar and have been attributed to basal sapping by diffuse ground-water flow (Wells and Andriamihaja, 1993). As time progressed, the scallops continued to expand headward and sideways, leaving linear ridges between adjacent scallops. An additional reason that these linear ridges are preserved in areas between scallops is because the ground-water flow is diverted away from the ridges (Figs. 20a and 18a). The linear ridges observed in the Farafra area (Figs. 12 and 13) are

Downloaded from gsabulletin.gsapubs.org on December 30, 2009

TABLE 2. PARAMETERS AND VALUES USED IN MODELING

Parameter	Value	Category
Independently known		
Critical discharge rate for sapping	0.002 m/day	Hydrology
Cell size (dimension of each cell)	170 m	Initial condition
Hydraulic conductivity	0.1 m/day	Hydrology
Storage coefficient	0.2 (dimensionless)	Hydrology
Fracture direction	5°	Initial condition
Rainfall as a function of time	Scaled by $\delta^{18}O$ record	Climate
Model derived		
Shale erodibility	0.04 (dimensionless)	Lithology
Limestone erodibility	0.0004 (dimensionless)	Lithology
Tufa erodibility	0.0004 (dimensionless)	Lithology
Sediment erodibility	0.08 (dimensionless)	Lithology
Sapping erosion scale factor	50.0 (dimensionless)	Hydrology
Tufa generation scale factor	0.001 (dimensionless)	Hydrology
Grid size (number of cells)	100×200	Initial condition
Slope of initial topography	1% (dimensionless)	Initial condition
Hydraulic conductivity in fractures	0.2 m/day	Hydrology

Note: The erodibilities were listed under model-derived group, but they were determined by comparing model results with independently measured denudation rates.

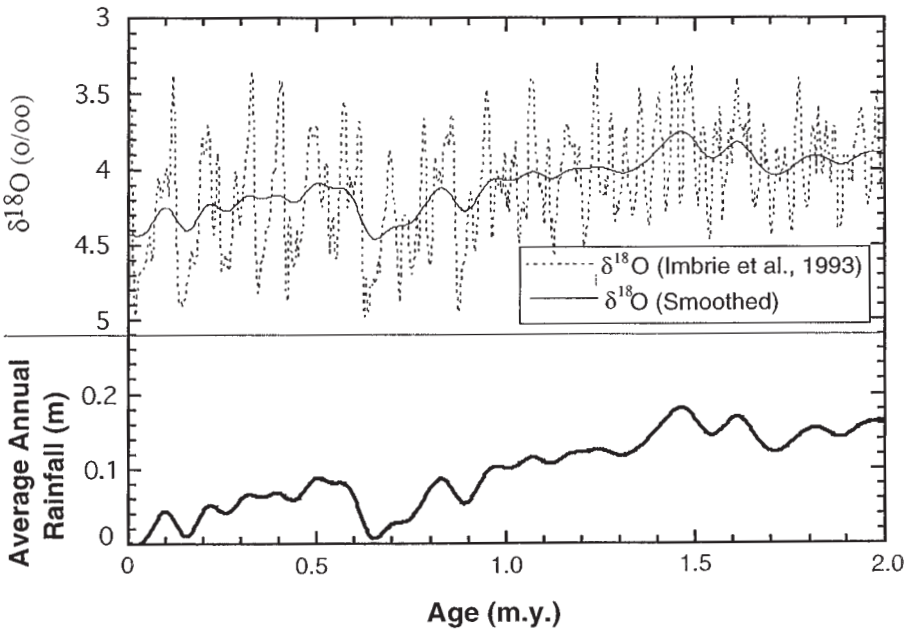

Figure 16. Average annual rainfall function (bottom) as defined from the composite deep-sea core $\delta^{18}O$ record (top, Imbrie et al., 1993). Also shown in top panel is the smoothed version of the $\delta^{18}O$ record, which is used to scale the changing climate rainfall function. The smoothed version was obtained by taking a three-point average of the original data consecutively for 200 times.

most likely formed by the same processes. The isolated inselbergs in the depressions are remnants of ridges. As noted by Dunne (1990) and Howard (1988), there was strong competition for ground-water among sapping features. Only three mature scallops developed out of the nine initial small scallops at the escarpment (Fig. 20a).

Model runs show that the model is very sensitive to critical discharge and that it controls the morphology of the scallops: the higher the critical discharge, the more elongated the scallop (Fig. 21). This is because the high critical discharge can only be satisfied at the scallop head, where the water table is the steepest. The positive feedback mechanism causes more headward retreat than lateral retreat. The higher critical discharge rate physically represents sapping conditions for rocks more resistant to failure (e.g., sandstones), because higher ground-water discharges are needed to mobilize them. The modeling results are consistent with the observations and interpretations in Egypt. Bedrock type controls morphology. The sandstone caprock of the southwestern El Quss Abu Said Plateau (Fig. 13) is more resistant to sapping, whereas the limestone caprock of the eastern part of the plateau (Fig. 12) is more susceptible to sapping. The scarp form of the Gilf Kebir Plateau (southwest of the study area), which is capped by ferruginized sandstone, is much more "channelized" than the limestone-capped plateau (Maxwell, 1982; Higgins, 1990), similar to the southern escarpment in the Farafra region.

For the model with fractures (Fig. 20b), erosion was concentrated preferentially along fracture zones due to higher ground-water discharge rates and therefore more sapping erosion. This process disrupted the natural development of scallops and formed channel systems in the limestone that followed structural trends (Fig. 20b), as observed in El Rufuf Pass area (Fig. 6). Tufa deposits were preferentially deposited along the fractures, because sapping erosion tapped into the ground-water table along high conductivity zones and generated springs. This situation is consistent with observations in Kharga and Kurkur. Less tufa was generated in the model with fractures as compared with the model with no fractures because higher discharge lowered the water table so that there were fewer springs to generate tufa deposits. The older tufas were preserved in the channels on the plateau as the climate became dry, and there was not enough erosion power to remove them. The vertical erosion rate and scarp retreat rate also decreased with time (Fig. 17b). The present values are about 7 times lower than those 1–2 m.y. ago. The erosions with fractures are generally lower than those with no fractures, because erosions were concentrated in the fracture zones. Figure 18b shows that ground-water flow is concentrated toward the scallop depressions and fracture zones.

The U/Th ages for samples with greater than 75% micrite (reliable ages, Sultan et al., 1996; Crombie et al., 1995, 1997) are shown in histogram form in Figure 19a in 20 k.y. increments. Also shown in Figure 19 are histograms of model ages for the oldest tufas preserved over the past million years. The histograms of the $\delta^{18}O$-forced changing climate models (Fig. 19, b and c) are consistent with the U/Th tufa age histogram (Fig. 19a). The younger peaks in the no-fracture case (Fig. 19b) are mainly from tufas forming in the scallops as the scallops tapped into the ground-water table and generated springs. These peaks also mimic the input rainfall function, i.e., $\delta^{18}O$ record (Figs. 19b and 16). Thus, the model not only simulates the first-order geomorphic features and deposits, but also generates similar tufa ages. In addition, the model results show that a majority of the tufas generated during older wet episodes were eroded away, but there may be tu-

Downloaded from gsabulletin.gsapubs.org on December 30, 2009

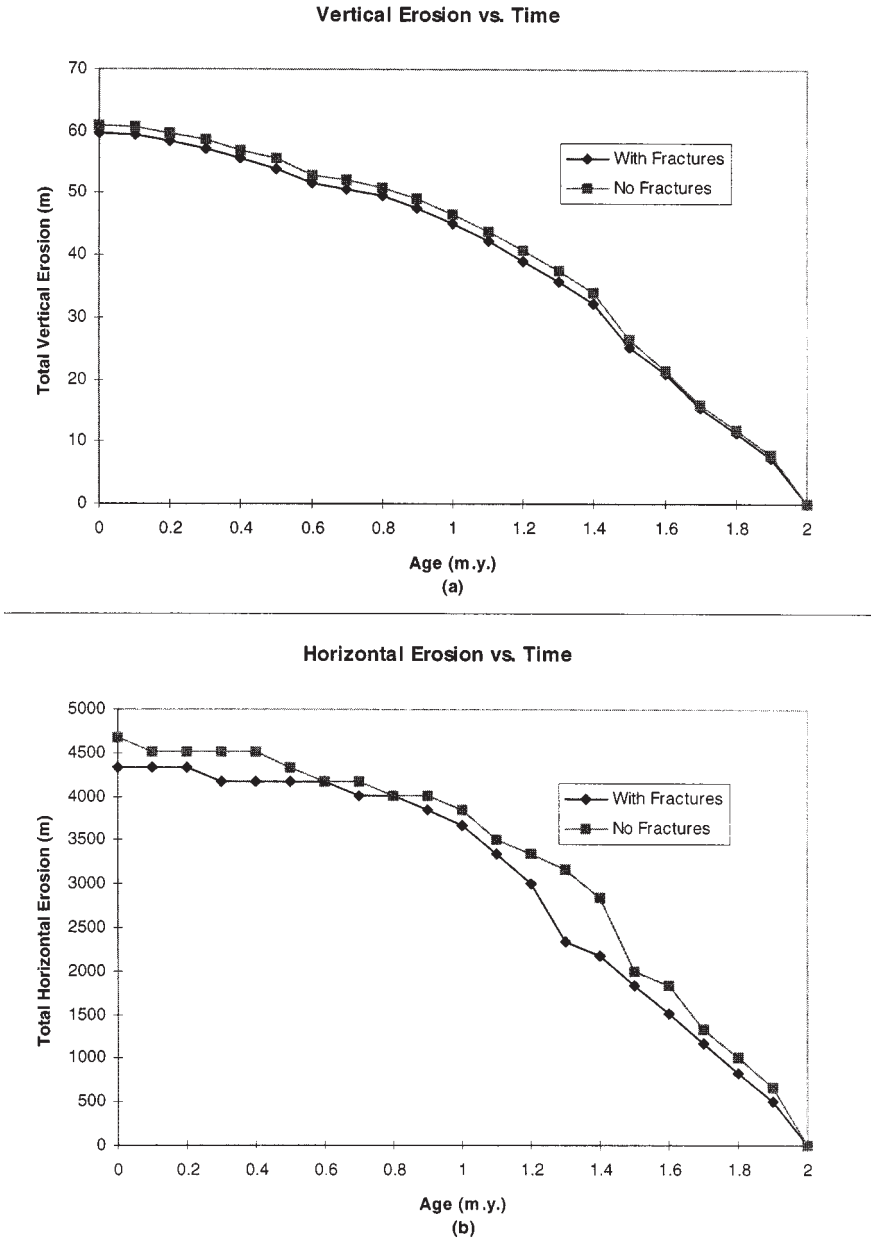

Figure 17. (a) Vertical surface erosion vs. time. (b) Horizontal scarp retreat vs. time. The erosion and retreat are calculated at the outcrop of the boundary between limestone and shale. The slopes of the lines are rates of erosion or retreat. Note the decrease in rates in both cases. Present is 0 m.y.

fas older than the U/Th detection limit (≈300 ka) that survived the erosion. Dating techniques that go beyond the U/Th limit will reveal more information about the paleoclimatic changes that are probably locked in these sediments.

CONCLUSIONS

Remote sensing and field observations demonstrate that differential erosion between friable shales and resistant limestones, ground-water sapping, associated slumping, and escarpment retreat are responsible for the generation and modification of the escarpments in the Western Desert of Egypt. This paper provides a predictive model that replicates the first-order morphology of escarpments by simulating coupled surface fluvial processes and ground-water sapping with geologically reasonable parameters. Observations and simulations also indicate that the scarp retreat rate is controlled by climatic conditions and has decreased as the climate changed from wet to hyperarid.

Simulations also provide insights into the details of ground-water sapping processes. Scalloped escarpment edges are the result of concentration of ground-water flow lines toward local depressions and mass wasting of the overlying rocks as the underlying shales are weakened by ground-water saturation. The competition for ground-water, the positive feedback mechanism, and structural controls contribute to the final morphology of the scallops. Ground-water sapping is dominant on the more permeable limestone units, forming characteristic sapping channels and scallops at the plateau edge, whereas surface runoff dominates on the impermeable shale units and forms the pediment and alluvial-fan systems. The model also predicts ages of preserved spring-derived tufa deposits. Simulations and U/Th ages of tufa samples indicate that the tufa-forming recharge events are episodic, consistent with the deep-sea core $\delta^{18}O$ paleoclimatic record and wetter periods that correlate with interglacial times. Furthermore, the $\delta^{18}O$-forced model replicates the changes toward arid conditions in northeastern Africa, with current fluvial and sapping rates that are much lower currently than 1 to 2 m.y. ago.

ACKNOWLEDGMENTS

This work was supported by National Aeronautics and Space Administration Geology Program grant 1358 to Washington University. We thank Stephen G. Wells, Ted A. Maxwell, and an anonymous reader for reviews. We also thank Roger J. Phillips, who kindly provided the Silicon Graphics system for running the simulations.

REFERENCES CITED

Albritton, C. C., Jr., Brooks, J. E., Issawi, B., and A. Awedan, 1990, Origin of the Qattara depression, Egypt: Geological Society of America Bulletin, v. 102, p. 952–960.

Baker, V. C., 1988, Evolution of valleys dissecting volcanoes on Mars and Earth, *in* Howard, A. D., Kochel, R. C., and Holt, H. E., eds., Sapping features of the Colorado plateau, a comparative planetary geology field guide: Washington D. C., National Aeronautics and Space Administration Special Publication 491, p. 96–97.

Baker, V. C., 1990, Spring sapping and valley network development, with case studies by Kochel, R. C., Baker, V. R., Laity, J. E., and Howard, A. D., *in* Higgins, C. G., and Coates, D. R., eds., Groundwater geomorphology: The role of subsurface water in earth-surface processes and landforms: Geological Society of America Special Paper 252, p. 235–265.

Ball, J., 1927, Problems of the Libyan desert: Geographical Journal, v. 70, p. 209–214.

Bear, J., 1972, Dynamics of fluids in porous media: New York, Elsevier Science, 764 p.

Berner, E. K., and Berner, R. A., 1987, The global water cycle: Geochemistry and environment: Englewood Cliffs, New Jersey, Prentice-Hall, 397 p.

Bras, R. L., 1990, Hydrology an introduction to hydrologic science: Reading, Massachusetts, Addison-Wesley, 643 p.

Brinkmann, P. J., Heinl, M., Hollaender, R., and Reich, G., 1987, Retrospective simulation of groundwater flow and transport in the Nubian aquifer system: Berliner Geowissenshaftler Abhandlung, Reihe A/Band 75.2, p. 465–516.

Brookes, I. A., 1993, Geomorphology and quaternary geology of the Dakhla oasis region, Egypt: Quaternary Science Reviews, v. 12,

Downloaded from gsabulletin.gsapubs.org on December 30, 2009

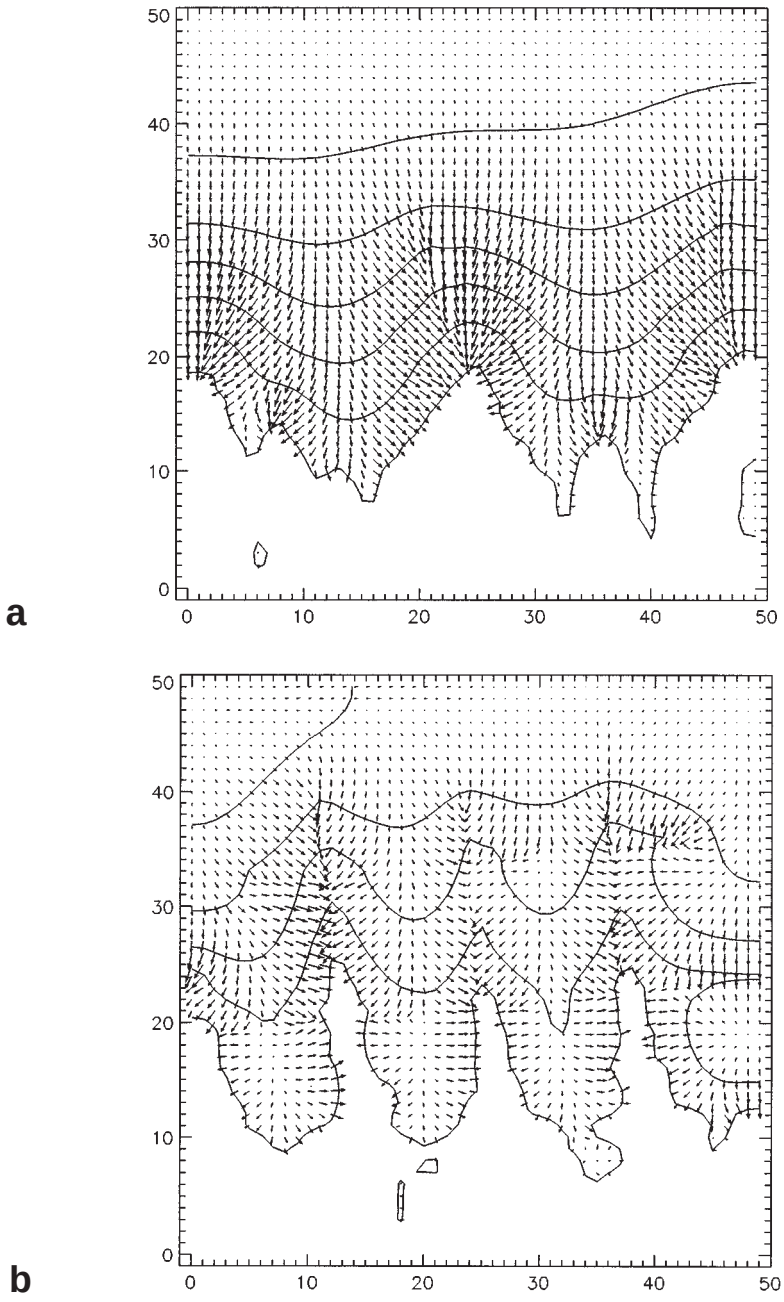

Figure 18. Ground-water flowlines and contours at 0.8 m.y. in time. The grid is resampled to half resolution for clarity (otherwise arrows clutter together) and only the active ground-water cells of the grid are shown. The numbers along x and y axes identify the columns and rows of the resampled grid. (Each dimension is 17 km.) The outcrop of the original contact boundary between limestone and shale is along the x axis of the figure. The areas filled with arrows are limestone and the white areas are exposed shales. (a) With no fractures. Ground-water flowlines converge toward the scallop depressions and diverge away from the ridges between scallops. (b) With fractures. Flowlines not only converge toward scalloped depressions, but also concentrate toward the fracture zones.

p. 529–552.
Caine, N., 1980, The landslide intensity-duration control of shallow landslides and debris flows: Geografiska Annaler, v. 62A, p. 23–27.
Caton-Thompson, G., and Gardner, E. W., 1932, The prehistoric geography of Kharga oasis: Geographical Journal, v. 80, p. 369–409.
Chase, G. C., 1992, Fluvial landsculpting and the fractal dimension of topography: Geomorphology, v. 5, p. 39–57.
Clemens, S., Prell, W., Murray, D., Shimmield, G., and Weedon, G., 1991, Forcing mechanisms of the Indian Ocean monsoon: Nature, v. 353, p. 720–725.
Crombie, M. K., Arvidson, R. E., Sturchio, N. C., Sultan, M., Alfy, Z. E., and Zeid, K. A., 1995, Paleoclimatic inferences from Travertine deposits, Kurkur Oasis, Western Desert, Egypt [abs.]: Eos (Transactions, American Geophysical Union), v. 76, p. S114.
Crombie, M. K., Arvidson, R. E., Sturchio, N. C., Sultan, M., Alfy, Z. E., and Zeid, K. A., 1997, Pleistocene pluvial episodes in the Western Desert, Egypt: Palaeogeography, Palaeoclimatology, Palaeoecology (in press).
Dawson, A. G., 1992, Ice age Earth: Late Quaternary geology and climate: London, New York, Routledge, 293 p.
Defense Mapping Agency Topographic Center, 1972, El Kharga, Egypt: Topographic map of Kharga: Washington, D.C., series 1501, NG36-9, scale 1:250 000, 1 sheet.
Domenico, P. A., and Schwartz, F. W., 1990, Physical and chemical hydrology: New York, John Wiley & Sons, 824 p.
Dunne, T., 1990, Hydrology, mechanics, and geomorphic implications of erosion by subsurface flow, *in* Higgins, C. G., and Coates, D. R., eds., Groundwater geomorphology; the role of subsurface water in earth-surface processes and landform: Geological Society of America Special Paper 252, p. 1–28.
El Aref, M. M., Khadrah, A. M. A., Lofty, Z. H., 1987, Karst topography and karstification processes in the Eocene limestone plateau of the El Bahariya oasis, Western Desert, Egypt: Zeitschrift für Geomorphologie, v. 31, p. 45–64.
Gilchrist, A. R., and Summerfield, M. A., 1992, Differential denudation and flexural isostasy in formation of rifted-margin upwarps: Nature, v. 346, p. 739–742.
Gindy, R. A., 1991, Origin of the Quattara Depression, Egypt: Discussion and Reply: Geological Society of America Bulletin, v. 103, p. 1734–1736.
Handley, H., List, F. K., and Pohlmann, G., 1987, eds., Geological map of Egypt, NG 36 SW Luxor: Egyptian General Petroleum Corporation/Conoco, scale 1:500 000, 1 sheet.
Haynes, C. V., 1982, The Darb El-Arab'in Desert: A product of Quaternary climatic change, *in* El-Baz, F., and Maxwell, T. A., eds., Desert landforms of southwest Egypt: A basis for comparison with Mars: Washington, D.C., National Aeronautics and Space Administration CR-3611, p. 91–117.
Haynes, C. V., Jr., 1987, Holocene migration rates of the Sudano-Sahelian Wetting Front, Arba'in Desert, eastern Sahara, *in* Close, A., ed., Prehistory of arid northern Africa: Dallas, Southern Methodist University Press, p. 69–84.
Hermina, M., 1990, The surroundings of Kharga, Dakhla and Farafra oases, *in* Said, R., ed., The geology of Egypt: Rotterdam, Netherlands, Balkema, p. 259–292.
Hesse, K. H., Hissene, A., Kheir, O., Schnacker, E., Schneider, M., and Thorweihe, U., 1987, Hydrogeological investigations in the Nubian aquifer system, eastern Sahara: Berliner Geowissenshaftler Abhandlung, Reihe A/Band 75.2, p. 397–464
Higgins, C. G., 1990, Seepage-induced cliff recession and regional denudation, with case studies by Osterkamp, E. R., and Higgins, C. G., *in* Higgins, C. G., and Coates, D. R., eds., Groundwater geomorphology: The role of subsurface water in earth-surface processes and landforms: Geological Society of America Special Paper 252, p. 291–317.
Howard, A. D., 1988, Groundwater sapping experiments and modeling, *in* Howard, A. D., Kochel, R. C., and Holt, H. E., eds., Sapping features of the Colorado plateau, a comparative planetary geology field guide: Washington, D.C., National Aeronautics and Space Administration Special Publication 491, p. 71–83.
Howard, A. D., 1994, Simulation modeling and statistical classification of escarpment planforms: Geomorphology, v. 12, p. 281-297.
Imbrie, J., and Imbrie, J. Z., 1980, Modeling the climate response to orbital variations: Science, v. 207, p. 943–953.
Imbrie, J., and 18 others, 1993, On the structure and origin of major glaciation cycles, 2. The 100,000 year cycle: Paleoceanography, v. 8, p. 669–735
Issar, A., 1982, Emerging groundwater: A triggering factor in the formation of the Makhteshim (erosion cirques) in the Negev and Sinai: Israel Journal of Earth Sciences, v. 32, p. 53–61.
Iverson, R. M., and Major, J. J, 1986, Groundwater seepage vectors and the potential for hillslope failure and debris flow mobilization: Water Resource Research, v. 22, no. 11, p. 1543–1548.
Iverson, R. M., and Major, J. J, 1987, Rainfall, groundwater flow, and seasonal movement at Minor Creek landslide, northwestern California: Physical interpretation of empirical relations: Geological Society of America Bulletin, v. 99, p. 579–594.
Klitzsch, E., List, F. K., and Pohlmann G., 1987, eds., Geological map of Egypt, 1987, NG 35 NE Farafra: Egyptian General Petroleum Corporation/Conoco, scale 1:500 000, 1 sheet.
Kochel, R. C., and Piper, J. F., 1986, Morphology of large valleys on Hawaii: Evidence for groundwater sapping and comparisons with Martian valleys: Journal of Geophysical Research, v. 91, p. E175–E192.
Kowalski, K., Van Neer, W., Szyndlar, Z., Gautier, A., Close, A. E., and Wendorf, F., 1989, A last interglacial fauna from Eastern Sahara: Quaternary Research, v. 32, p. 335–341.
Laity, J. E., 1988, The role of groundwater sapping in valley evolution on the Colorado Plateau, *in* Howard, A. D., Kochel, R. C., and Holt, H. E., eds., Sapping features of the Colorado plateau, a comparative planetary geology field guide: Washington, D.C., National Aeronautics and Space Administration Special Publication 491, p. 63–70.
Laity, J. E., and Malin, M. C., 1985, Sapping processes and the development of theater-headed valley networks on the Colorado plateau: Geological Society of America Bulletin, v. 96, p. 203–217.
Larsen, M. C., and Simon, A., 1993, A rainfall intensity-duration thresh-

Downloaded from gsabulletin.gsapubs.org on December 30, 2009

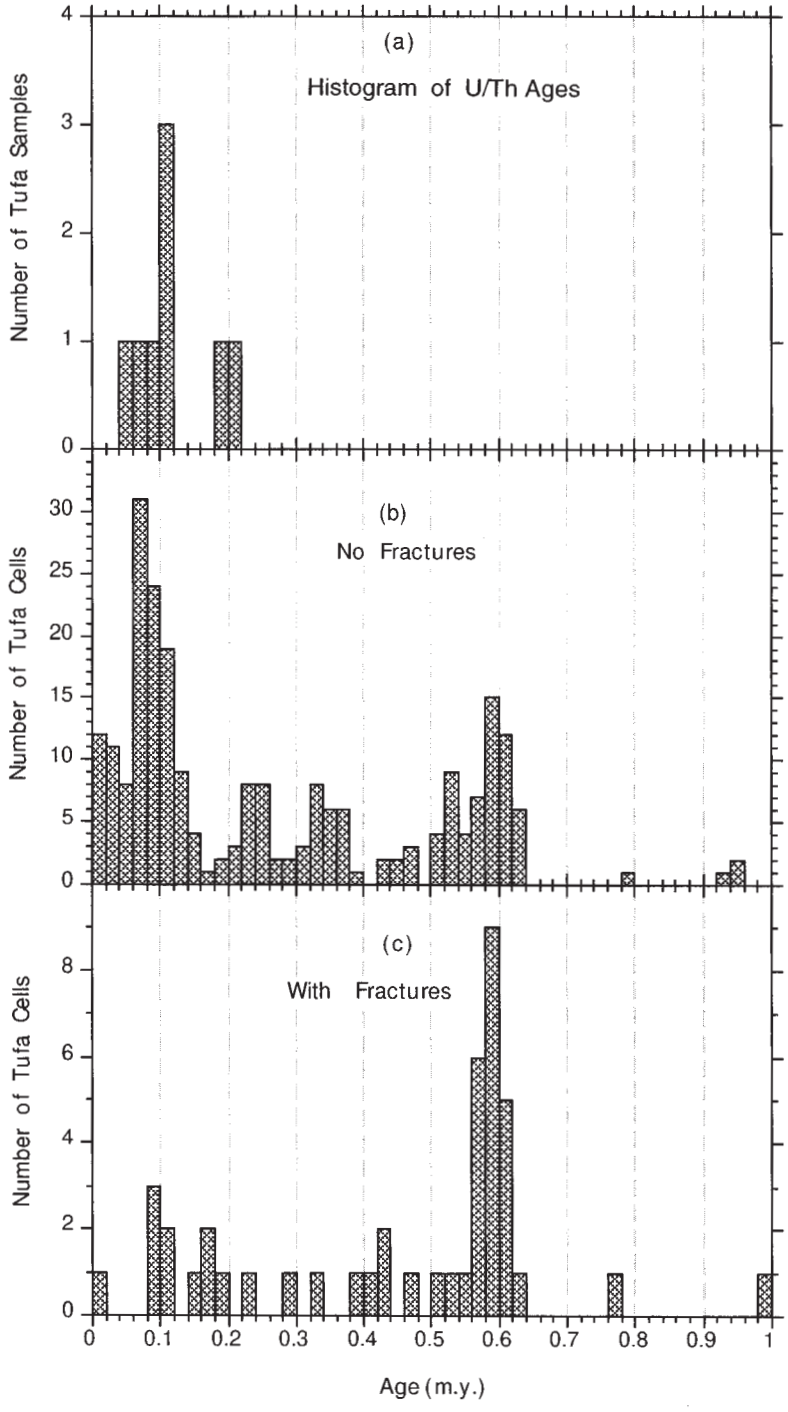

Figure 19. U/Th ages of tufas from the Farafra (1 sample) and Kurkur (7 samples) areas are shown in histogram (a). Model tufa age histograms for $\delta^{18}O$-forced changing climate (b and c) are aligned vertically for comparison. The $\delta^{18}O$-forced models (b and c) produced tufa ages consistent with U/Th ages. Note that the scales of the y axes are different. U/Th data from Sultan et al. (1996) and Crombie et al. (1995, 1997).

old for landslides in a humid-tropical environment: Puerto Rico, Geography Annals, v. 75A, p. 12–23.
Luo, W., 1995, Computer simulation of landform evolution, Western Desert, Egypt and paleoclimate implications [Ph.D. dissert.]: St. Louis, Missouri, Washington University, 275 p.
Maxwell, T. A., 1982, Erosional patterns of the Gilf Kebir plateau and implications for the origin of Martian Canyonlands, *in* El-Baz, F., and Maxwell, T. A., eds., Desert landforms of southwest Egypt: A basis for comparison with Mars: Washington, D.C., National Aeronautics and Space Administration CR-3611, p. 281–300.
McCauley, J. F., Breed, C. S., and Groler, M. J., 1982, The interplay of fluvial, mass-wasting and aeolian processes in the Eastern Gilf Kebir region, *in* El-Baz, F., and Maxwell, T. A., eds., Desert landforms of southwest Egypt: A basis for comparison with Mars: Washington, D.C., National Aeronautics and Space Administration CR-3611, p. 207–239.
McCauley, J. F., Breed, C. S., Schaber, G. G., McHugh, W. P., Issawi, B., Haynes, C. V., Groler, M. J., and El Kilani, A., 1986, Paleodrainages of the eastern Sahara: The radar river revisited (SIR-A/B implications for a mid-Tertiary trans-African drainage system): IEEE, Transactions on Geoscience and Remote Sensing, v. GE-24, p. 624–648.
Nicholson, S. E., and Folhn, H., 1980, African environmental and climatic changes and the general atmospheric circulation in late Pleistocene and Holocene: Climatic Change, v. 2, p. 313–348.
Pavich, M. J., 1985, Appalachian piedmont morphogenesis: Weathering, erosion, and Cenozoic uplift, *in* Morisawa, M., and Hack, J. T., eds., Tectonic geomorphology: Boston, Allen and Unwin, p. 299–319.
Prell, W. L., and Kutzbach, J. E., 1987, Monsoon variability over the past 150,000 years: Journal of Geophysical Research, v. 92, p. 8411–8425.
Rossignol-Strick, M., 1985, Mediterranean Quaternary sapropels: An immediate response of the African monsoon to variation[s?] of insolation: Palaeogeography, Palaeoclimatology, Palaeoecology, v. 49, p. 237–263.
Said, R., 1962, The geology of Egypt: Amsterdam, New York, Elsevier, 377 p.
Said, R., 1983, Remarks on the origin of the landscape of the eastern Sahara: Journal of African Earth Sciences, v. 1, p. 153–158.
Said, R. 1990, Quaternary, *in* Said, R., ed., The geology of Egypt: Rotterdam, Netherlands, Balkema, p. 487–507.
Schumm, S. A., Boyd, K. F., Wolff, C. G., and Spitz, W. J., 1995, A ground-water sapping landscape in the Florida Panhandle: Geomorphology, v. 12, p. 281–297.
Selby, M. J., 1993, Hillslope materials and processes (Second edition): Oxford, Oxford University Press, 451 p.
Street-Perrott, F. A., and Harrison, S. P., 1984, Temporal variations in lake levels since 30,000 yr B.P.: An index of the global hydrological cycle, *in* Hansen, J. E., and Takahashi, T., eds., Climate processes and climate sensitivity: Washington, D.C., American Geophysical Union Geophysical Monograph Series, v. 29, p. 118–129.
Stringfield, V. T., LaMoreaux, P. E., LeGrand, H. E., Tolson, J., and Rayfield, C. R., 1974, Karst and paleohydrology of carbonate rock terrains in semiarid regions, with a comparison to humid karst of Alabama: Geological Survey of Alabama Bulletin, v. 105, 106 p.
Sultan, M., Sturchio, N., Hassan, F., Hamdan, M. A., Mahmood, A. M., and El Alfy, Z., 1996, New constraints on the Quaternary paleoclimate of North Africa: Cairo, Egypt, Geological Survey of Egypt, Abstracts of the Centential Meeting (Nov. 19–22/1996) of the Geological Survey of Egypt, p. 192–193.
Szabo, B. J., Haynes, C. V., and Maxwell, T. A., 1995, Ages of Quaternary pluvial episodes determined by uranium-series and radiocarbon dating of lacustrine deposits of eastern Sahara: Palaeogeography, Palaeoclimatology, Palaeoecology, v. 113, p. 227—242.
Thomas, M. F., 1994, Ages and geomorphic relationships of saprolite mantles, *in* Robinson, D. A., and Williams, R. B. G, eds., Rock weathering and landform evolutions: New York, John Wiley and Sons, p. 287–301.
Thompson, B. W., 1965, The climate of Africa: New York, Oxford University Press, 300 p.
Uchupi, E., and Oldale, R. N., 1994, Spring sapping origin of the enigmatic relict valleys of Cape Cod and Martha's Vineyard and Nantucket Islands, Massachusetts: Geomorphology, v. 9, p. 83–95.
Van Zinderen Bakker, E. M., and Mercer, J. H., 1986, Major late Cenozoic climatic events and paleoenvironmental changes in Africa viewed in a world wide context: Palaeogeography, Palaeoclimatology, Palaeoecology, v. 56, p. 217–235.
Wang, H. F., and Anderson, M. P., 1982, Introduction to groundwater modeling finite difference and finite element methods: New York, Freeman and Company, 237 p.
Wells, N. A., and Andriamihaja, B., 1993, The initiation and growth of gullies in Madagascar: Are humans to blame?: Geomorphology, v. 8, p. 1–46.
Wendorf, F., and Schild, R., 1980, Prehistory of the eastern Sahara: New York, Academic Press, 414 p.

MANUSCRIPT RECEIVED BY THE SOCIETY AUGUST 4, 1995
REVISED MANUSCRIPT RECEIVED APRIL 29, 1996
MANUSCRIPT ACCEPTED JUNE 29, 1996

Downloaded from gsabulletin.gsapubs.org on December 30, 2009

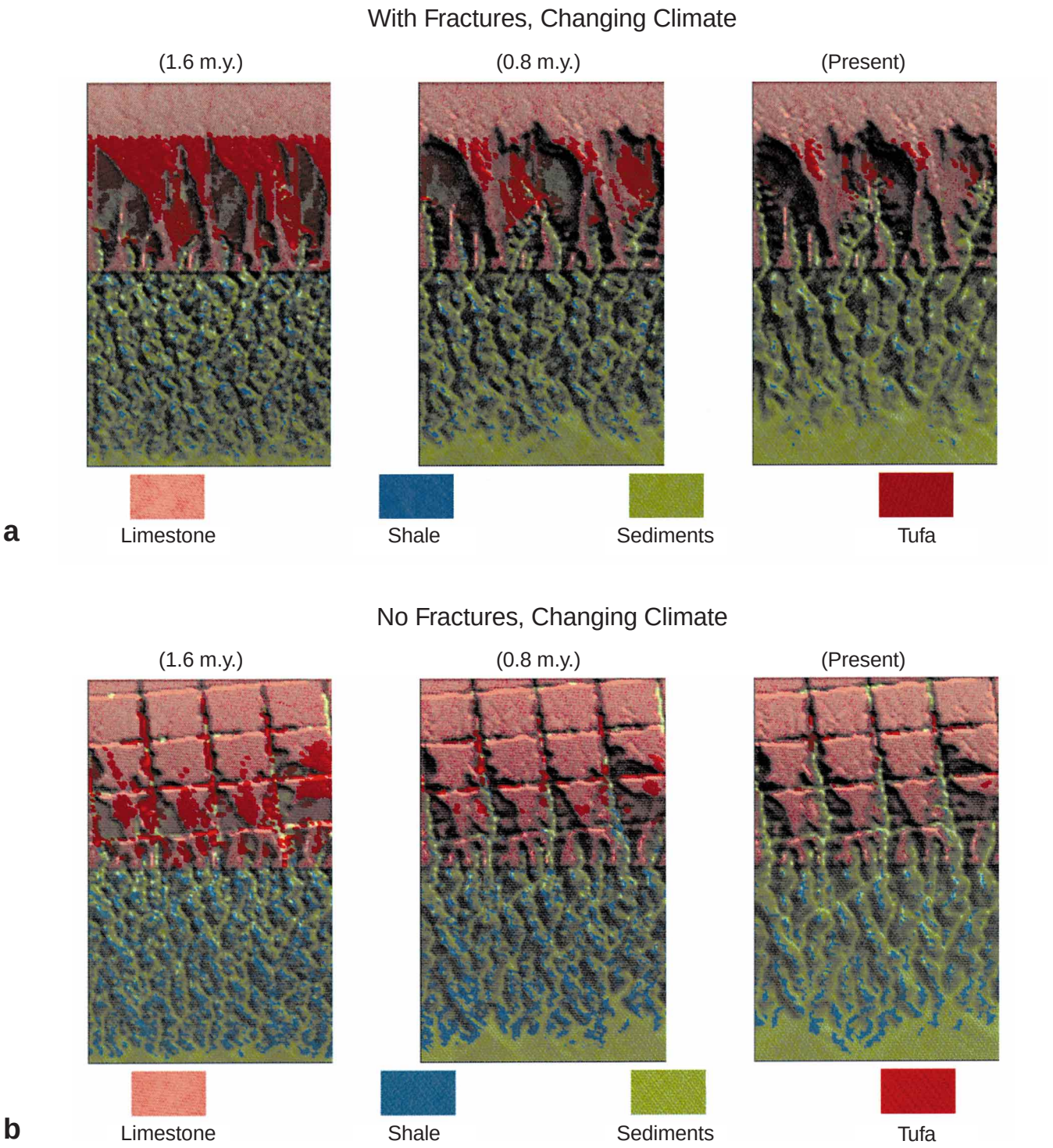

Figure 20. Resultant topography of modeling shown at 1.6, 0.8, and 0 m.y. in time. The viewing angle is from top and light source is from the southeast, similar to the sun angle when satellite images were taken. Pink is limestone, blue-green is shale, yellow is sediment, and red is spring-derived tufa. (a) Without fractures. The escarpment formed at the outcrop of the contact between limestone and shale. Scallop-shaped local depressions started at the escarpment and expanded headward and sideways. Pediment covered with sediments formed in the shale close to the escarpment and coalescing alluvial fans or bajada plains formed in the distal portion of shales. Linear ridges formed as adjacent scallops expanded. Each scallop formed its own drainage system emanating from the base of the escarpment. Tufas deposited on the plateau at earlier time were nearly eroded away; some were preserved on the plateau between scallops. Younger tufas were preserved in the scallops. (b) With fractures. Erosion preferentially occurred along the fractures and formed channels along structural trends. The scallop-shaped local depressions seen in the no-structure cases were disrupted. Tufa deposits are mostly found along fractures and at the intersection of the fractures.

Downloaded from gsabulletin.gsapubs.org on December 30, 2009

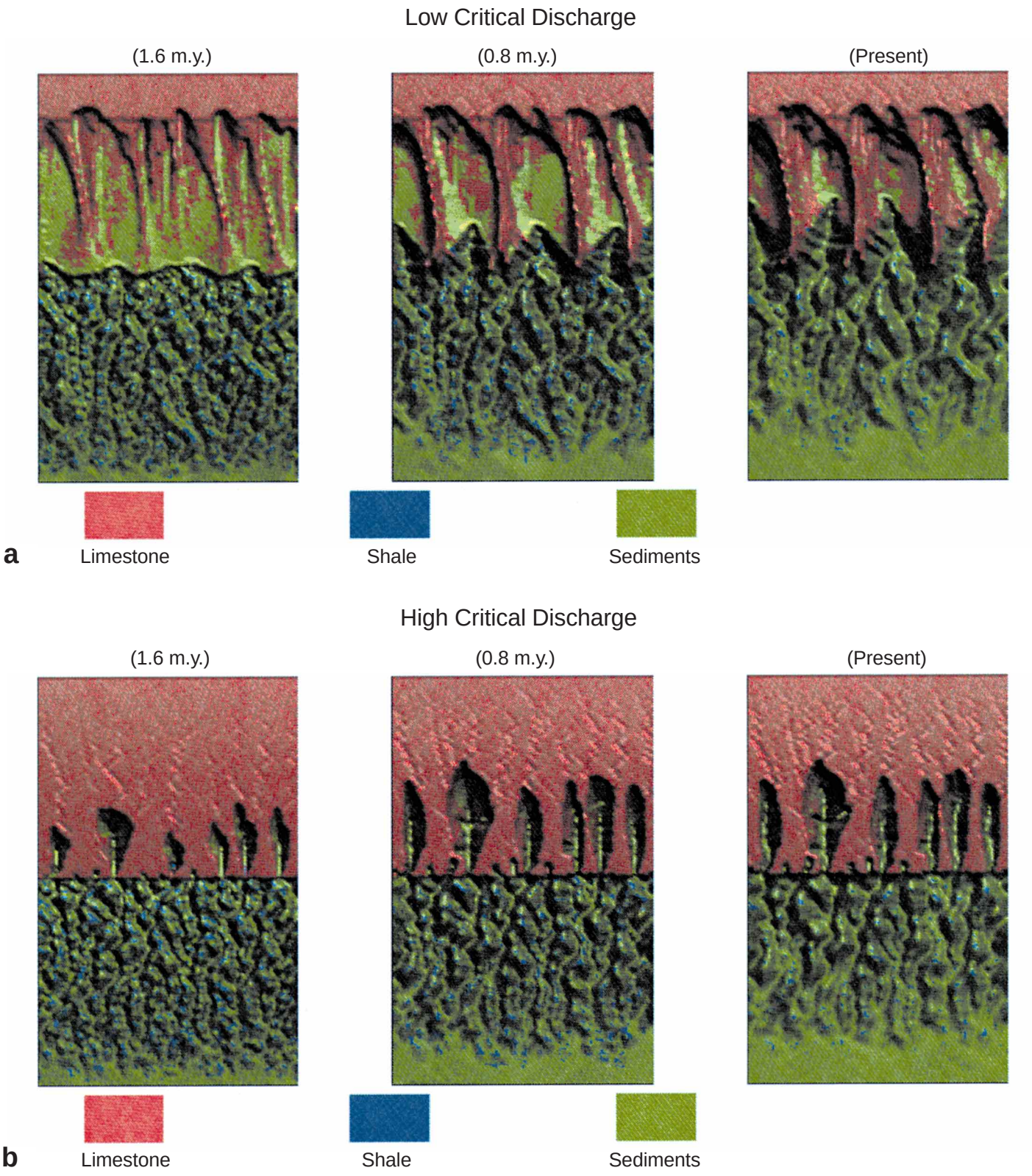

Figure 21. Sensitivity test of critical discharge. Viewing angle and color coding are the same as those in Figure 17. Tufa deposits are not shown to emphasize the morphology. (a) Critical discharge (0.001 m/day) lower than the independently determined value (0.002 m/day): scallops are wider and more open as compared with a higher value (b). (b) Critical discharge rate (0.004 m/day) higher than the independently determined value: scallops are narrower and more elongated. The ridges between adjacent scallops are also wider. Higher critical discharge represents a rock more resistant to sapping failure (e.g., sandstone). Simulation result is consistent with observation in Farafra.